Quantum field theory of atoms interacting with photons. III. Scattering of weak cw light from cold samples of bosonic atoms

L. You,[1] Maciej Lewenstein,[1,2] Roy J. Glauber,[3] and J. Cooper[4]

[1]*Institute for Theoretical Atomic and Molecular Physics, Harvard-Smithsonian Center for Astrophysics, 60 Garden Street, MS 14, Cambridge, Massachusetts 02138*

[2]*Centrum Fizyki Teoretycznej, Polska Akademia Nauk, 02-668 Warsaw, Poland*

[3]*Lyman Laboratory, Physics Department, Harvard University, Cambridge, Massachusetts 02138*

[4]*JILA, University of Colorado and National Institute of Standards and Technology, Boulder, Colorado 80309-0440*

(Received 13 June 1995)

We study the coherent scattering of weak light from a system of cooled bosonic atoms in a trap. We derive and discuss in detail the scattering equation for such a process that describes multiple scatterings from different atoms. Our theory accounts for atom-atom interactions and determines the density profile of the atomic fields from the self-consistent Bogoliubov-Hartree method. We present two kinds of analytic solutions to the scattering equation using the *on-shell approximation* and the *generalized diffraction theory*. We discuss the validity of those approaches, and demonstrate that they both lead to similar results. Our studies indicate that the scattering cross sections exhibit non-Lorentzian shapes with narrow features close to resonance. Coherent scattering occurs mainly in the forward direction, and the angular distribution is limited by the size of the atomic sample in the trap. We present results for various ranges of relevant parameters such as trap size, interaction strength, number of atoms, and temperature, etc.

PACS number(s): 03.75.Fi, 42.50.Fx, 32.80.−t

I. INTRODUCTION

This paper is the third in a series of papers devoted to the study of the quantum field theory of atoms interacting with photons. In the previous two papers we discussed the fundamentals of the theory (paper I [1]), and the problem of scattering of short laser pulses off trapped atomic samples (paper II [2]). The present work is devoted to a detailed study of the problem of weak cw light scattering from such systems. As we stressed in papers I and II, the experimental realization of Bose-Einstein condensates (BEC) [3] in systems of trapped and cooled atoms [4] has recently become one of the major efforts of atomic physics [5]. Significant progress has been achieved during the last year towards this goal. Three groups [6] now have reported observation of evaporative cooling [7] in cold (laser precooled) alkali-metal systems. New techniques have also been developed to cool spin-polarized hydrogen [8]. Thus, it is becoming urgent to consider in detail problems concerning detection and observation of a condensate, or more generally of a system of quantum statistically degenerate atoms.

Perhaps one of the most natural ways to detect BEC is by scattering light from the system of cooled atoms. Several authors have considered this problem in recent years. Quantum optical studies of light scattering from a BEC have been initiated by Svistunov and Shlyapnikov [9], and Politzer [10]. They discussed the problem of scattering of weak light from a condensate at low temperatures $T \simeq 0$, and considered the case of a spatially homogeneous gas. Such a case corresponds physically to the limit of a (formally) infinitely large trap. In this limit atomic and photonic degrees of freedom mix, giving rise to the formation of *polariton*-type excitations and a gap in the excitation spectrum close to resonance. This theory can be extended to the case of atoms inside finite-size traps. In particular, for traps that have a slab geometry or sharp boundaries, one expects that because of the gap in the spectrum, resonant light will not be able to propagate inside the condensate, and therefore will be strongly reflected back from the boundary of the condensate. In practice, the gap appears only in the narrow line limit, i.e., when the width of the gap significantly exceeds the spontaneous emission rate γ. Javanainen considered another limiting case of an optically thin condensate [11], with size a of the order of the resonant wavelength λ. His approach consists essentially of replacing the atomic field (which has infinite degrees of freedom) by a single harmonic oscillator in the limit of low optical density. This harmonic oscillator describes collective excitations of the condensate. Within this framework one can show that the scattering will take place mainly in the forward direction, and the scattering cross section will have a Lorentzian line shape with a width proportional to the collective (superradiant) spontaneous emission rate (which typically would be of the order of $\gamma n \lambda^2 a$, where n is the atomic density). In a recent paper [12] we have argued that the above conclusions would be modified in a trap of significant optical thickness, with no sharp boundaries, and of finite size a in the range of $(1–20)\lambda$. In the case of moderate atomic densities, n such that $n(\lambda/2\pi)^3 \simeq 1–10$, one does not observe backscattering or effects directly related to polariton formation. The physical reason is that the effective gap in the excitation spectrum is narrow in this regime, so that its effects are washed out by various mechanisms of line broadening for individual atoms. On the other hand, the propagation effects influence the scattering process in such a way that the approach of Ref. [11] also becomes less adequate. Although the large scale width of the spectrum remains the same as predicted in [11], the spectrum becomes non-Lorentzian and exhibits a narrow peak at the resonance. The width of this narrow feature is controlled by the dominant single-atom dissipative and dephasing processes such as

spontaneous emission to noncondensed states, or quantum diffusion of the excited atomic wave packets [12]. Weak light scattering in the ultralow density limit has also been studied by Gajda and Mostowski [13] (see also [14]) using the Born approximation.

All of the above papers concern the problem of *coherent* scattering; that is, they concentrate on the evaluation of the mean elastically scattered field. Coherent scattering is a probe of the density of the system, and in this sense is not necessary specific for Bose-Einstein statistics. The quantum statistical character of the atoms exhibits itself in coherent scattering only through the fact that at low temperatures the density profiles for bosonic or fermionic atoms are different. In order to obtain explicit effects of the statistics, one needs to calculate higher-order moments of the scattered field that will probe higher-order correlations of the atomic density. Considerable progress on this ambitious task has been recently realized by Morice, Castin, Dalibard [15], who studied the refractive index of a dilute Bose gas. These authors have carried out a density expansion of the refractive index in a homogeneous system up to second order, and effectively resummed a class of appropriate diagrams of the perturbation theory that account for the effects of photon exchange processes between pairs of atoms. The first nonzero correction to the index of refraction related to the statistical nature of atoms is found to be proportional to the density-density correlation function. Similar corrections are expected to arise in the *incoherent* spectrum of light scattered from the trapped atomic samples. In paper II we have in fact calculated incoherent spectra for the case of scattering of short laser pulses (see also [16]), and have shown that they provide a direct probe of the density-density correlations. In the present paper, however, we will concentrate on coherent scattering, and do not address the question of explicit quantum statistical effects [17].

The aim of this paper is to examine the problem of the coherent scattering of a weak cw laser field from a system of cold trapped atoms in detail. We discuss various limiting cases and relate them to the results known from other studies. Our starting point is a scattering equation valid in the weak-field limit (for its derivation, see paper I). We present two alternative analytic approaches to the solution of this equation: one based on the *on-shell* approximation to the scattering matrix [18], and the other based on Glauber's *generalized diffraction theory* (GDT) [19–21]. We calculate and discuss scattering cross sections, and their angular and spectral distributions for a wide range of parameters such as temperature, trap size, number of atoms, etc. We analyze also the effects related to atom-atom interactions.

Throughout this paper we focus our attention on the range of parameters describing contemporary magnetic traps such as developed by Monroe *et al.* [22] [cesium atoms, $\lambda \simeq 800$ nm, $a \simeq 1$–10 μm, trap frequency $\omega_t \simeq (2\pi)10$ Hz, $\gamma \simeq (2\pi)2.5$ MHz]. The paper is organized as follows. In Sec. II we present our model in the Fock representation. The model we consider belongs to class A (defined in paper I), i.e., a system where one neglects short-range atom-atom interactions. The model is idealized further by neglecting the spontaneous emission processes that lead to modifications of the atomic distribution in the ground electronic state. In particular at $T=0$ it neglects spontaneous emission to states other than the condensate. However, these restrictions will be lifted later in the paper. The general derivation of the scattering equation in the weak-field limit has been presented in paper I not only for class A models of noninteracting atoms, but also for class B and C models that account for atomic collisions. We have shown in particular that the scattering equation for the coherently scattered field depends functionally only on the mean density profile of atoms in thermal equilibrium. Here we include only a brief discussion of the derivation. In Sec. III we perform a detailed analysis of various limits of the self-energy kernel that enters the scattering equation. We also evaluate the kernel analytically in some cases for class A models. This analysis demonstrates clearly how the kernel can be reduced to a form fully determined by the mean atomic density.

Section IV is devoted to the evaluation of atomic density profiles for class C models that include the effects of atomic ground-ground interactions in thermal equilibrium. We again follow the procedure of paper I and calculate the equilibrium density of the condensate at $T=0$ using a self-consistent Bogoliubov-Hartree method [23,24]. This calculation consists of a numerical solution of the nonlinear Schrödinger equation describing the BEC ground-state wave function for atoms in a trap interacting via a zero-range effective potential. We present in this section some details of our numerical approach and the results. In Sec. V we present analytic solutions of the scattering equation in the on-shell approximation, and apply these solutions to calculate scattering and absorption cross sections as well as angular distributions of the scattered radiation. The advantage of using the on-shell approximation is that it allows us to perform explicit analysis of the solutions in terms of partial waves, and to discuss the relation to Javanainen's theory [11]. The disadvantage of this approach is that it does not appear to have a precisely defined regime of validity. Moreover, it also approximates the propagation between multiple scatterings by regarding it as a propagation of monochromatic photons. For these reasons, we present in Sec. IV an alternative solution to the scattering equation based on the GDT. The latter approach has several advantages. First, it is analytically simpler than the previous one. Second it is formulated in the spatial representation, and thus allows us to calculate spatial characteristics of the scattered field. In addition, the GDT accounts for off-shell propagation effects for photon wave vectors close to wave vector of incident laser field. Finally, the GDT has well-defined validity criteria that we check in Sec. VI.

In Sec. VII we present our numerical results. Both approximate theories give unexpectedly good agreement and predict a non-Lorentzian line shape with a narrow peak at resonance. In the idealized model the width of the narrow peak results from the effects of quantum diffusion and drift of the excited atomic wave packets. In a more realistic model this width becomes of the order of maximum of either the natural (γ) or the diffusive (Γ_d) linewidth (see discussion later). Scattering occurs mainly in the forward direction, and the angular divergence is determined by the size of the atomic sample. In fact, the distribution of the total field exhibits a dip in the most dense regions of the trap, that is to say it is deflected from the condensate without entering the central region. This resembles the effects due to the formation of a gap in the polariton spectrum discussed in Refs. [9]

and [10]. We discuss those results in various ranges of parameters, and in particular we study the role of atom-atom interactions by comparing the results for class A and C models.

The paper contains three appendices. In Appendix A, we outline the definitions for the scattering cross sections and the normalizations used. We also derive an optical theorem that will be used when computing the total cross section within the on-shell approximation. In Appendix B we discuss the problem of spontaneous emission out of the condensate using a Schrödinger equation approach. In Appendix C we discuss properties of the self-energy kernel at a finite temperature $T \neq 0$.

II. THE SCATTERING EQUATION

In this section we remind the readers of the essential steps in the derivation of the scattering equation valid in the weak-field limit. The details of this derivation for class A, B, and C models can be found in paper I. The discussion presented below focuses on the case of class A models that neglect short-range atom-atom interactions. We stress, however, that the final result applies equally well for other classes of models that incorporate effects of atomic collisions.

The Hamiltonian governing the interactions of light with N bosonic atoms confined in a trap takes the following second quantized form in the Fock representation [1]:

$$\begin{aligned}\mathscr{H} = & \sum_{\vec{n}} E^{g}_{\vec{n}} g^{\dagger}_{\vec{n}} g_{\vec{n}} + \sum_{\vec{m}} (E^{e}_{\vec{m}} + \omega_0) \vec{e}^{\dagger}_{\vec{m}} \vec{e}_{\vec{m}} \\ & + \sum_{\vec{n},\vec{m}} \sum_{\mu} \int d\vec{k} \rho(k) [\, \eta_{\vec{n}\vec{m}}(\vec{k}) g^{\dagger}_{\vec{n}} a^{\dagger}_{\vec{k}\mu} \vec{e}_{\vec{m}} \cdot \vec{\epsilon}_{\vec{k}\mu} + \text{H.c.}] \\ & + \sum_{\mu} \int d\vec{k} c k a^{\dagger}_{\vec{k}\mu} a_{\vec{k}\mu} . \end{aligned} \tag{1}$$

In Eq. (1) we have used the rotating-wave approximation, and have employed atomic units. We have also neglected the *contact* interaction terms [25]. The symbols $g_{\vec{n}}$, $g^{\dagger}_{\vec{n}}$ denote atomic annihilation and creation operators for the $\vec{n}$th state of the (electronic) ground-state trap potential. For a rotationally invariant potential, $\vec{n}$ is actually a triplet index (n_x, n_y, n_z). The corresponding energy is $E^{g}_{\vec{n}} = \omega_t (n_x + n_y + n_z)$ where ω_t is the frequency of the harmonic trap potential for the ground state. $\vec{e}_{\vec{m}}, \vec{e}^{\dagger}_{\vec{m}}$ denote atomic annihilation and creation operators in the excited-state trap potential. The corresponding energies are $E^{e}_{\vec{m}} + \omega_0$, i.e., are shifted by the electronic transition frequency. We consider here the case of a transition from an s state to a p state and therefore $\vec{e}_{\vec{m}}$'s and $\vec{e}^{\dagger}_{\vec{m}}$'s have a corresponding vector character. This is not the case of the transition in cesium ($6S_{1/2}, F=4$ to $6P_{3/2}, F=5$), but the character of the transition is not essential for our conclusions. $a_{\vec{k}\mu}$ and $a^{\dagger}_{\vec{k}\mu}$ denote the annihilation and creation operators for photons of the momentum $\vec{k}$ and linear polarization $\vec{\epsilon}_{\vec{k}\mu}$ ($\mu = 1,2$). All these operators fulfill standard bosonic commutation relations. The coupling $\rho(k)$ is a slowly varying function of k related to the natural linewidth (HWHM) $\gamma = (8\pi^2 k_0^2 / 3c) |\rho(k_0)|^2$, with $k_0 = \omega_0 / c$. Finally, $\eta_{\vec{n}\vec{m}}(\vec{k})$ is the Franck-Condon factor (i.e., matrix element for the center-of-mass transition from the $\vec{n}$th state of the ground-state potential to the $\vec{m}$th state of the excited-state potential),

$$\eta_{\vec{n}\vec{m}}(\vec{k}) = \langle g, \vec{n} | e^{-i\vec{k}\cdot\vec{R}} | e, \vec{m} \rangle . \tag{2}$$

The above Hamiltonian includes the strong resonant interactions due to electronic dipole-dipole forces and exchange of transverse photons [27,28]. For clarity of discussion we neglect at present other forces that are involved in atomic collisions.

As mentioned in paper I, there are several possible methods of deriving the scattering equation for the electromagnetic (EM) field in the limit of weak cw incident light field. One such method involves the Schrödinger equation approach, and assumes that at any time at most one photon is present. This assumption reduces the available Hilbert space to two manifolds of states: (i) the states in which all atoms are in the ground electronic state and the EM field is in a single photon state; (ii) the states in which all but one of the atoms are in the ground electronic state, one atom is excited, and the EM field is in the vacuum state. This approach is discussed in more detail in Appendix B, where we apply it to study the problem of spontaneous emission out of the condensate.

Another approach employs the Heisenberg equations of motion for all the operators involved. The disadvantage of this method is that the treatment of line broadening due to spontaneous emission events, which deforms the initial atomic distribution in the ground electronic state, becomes more complicated. On the other hand, if one neglects broadening by spontaneous emission out of the condensate from the excited electronic states, the Heisenberg equation approach treats the idealized model with a fixed initial atomic distribution as a closed (Hamiltonian) system. Such an idealized model includes line broadening effects due to the quantum diffusion and drift of the excited wave packets. One should stress that probing the system does not necessarily have to be done using the same wavelength as is used for cooling [which for cesium atoms correspond to $\lambda \simeq 800$ nm, $\gamma \simeq (2\pi) 2.5$ MHz]. In principle one could therefore employ other resonant transitions that are characterized by much narrower natural linewidths. In such situations the use of the idealized model would be much more valid, since the line broadening due to quantum diffusion and drift motion would exceed the natural broadening. We shall first discuss the idealized model, and account for other line broadening effects later.

The Heisenberg equations of motion that follow from the Hamiltonian (1) are

$$\dot{a}_{\vec{k}\mu} = -ick a_{\vec{k}\mu} - i\rho(k) \sum_{\vec{n},\vec{m}} g^{\dagger}_{\vec{n}} (\vec{e}_{\vec{m}} \cdot \vec{\epsilon}_{\vec{k}\mu}) \eta_{\vec{n}\vec{m}}(\vec{k}), \tag{3}$$

$$\begin{aligned}(\dot{\vec{e}}_{\vec{m}} \cdot \vec{\epsilon}_{\vec{k}\mu}) = & -i(E^{e}_{\vec{m}} + \omega_0) \vec{e}_{\vec{m}} - i \sum_{\mu'} \int d\vec{k}' \rho(k') \\ & \times \sum_{\vec{n}} a_{\vec{k}'\mu'} g_{\vec{n}} [\, \eta_{\vec{n}\vec{m}}(\vec{k}')]^{*} (\vec{\epsilon}_{\vec{k}'\mu'} \cdot \vec{\epsilon}_{\vec{k}\mu}), \end{aligned} \tag{4}$$

$$\dot{g}_{\vec{n}} = -iE^g_{\vec{n}} g_{\vec{n}} - i\sum_{\mu'} \int d\vec{k}\rho(k) \sum_{\vec{m}} a^\dagger_{\vec{k}\mu}(\vec{e}_{\vec{m}} \cdot \vec{\epsilon}_{\vec{k}\mu}) \eta_{\vec{n}\vec{m}}(\vec{k}). \tag{5}$$

For scattering of weak light we assume that initially all atoms are in the ground electronic state and in thermal equilibrium with respect to their center-of-mass motion. We expect that the weak incident field will not disturb this equilibrium significantly as only one single photon is scattered at a time. In particular, we also assume that the atomic distribution in the ground electronic state remains unchanged in the process of scattering. As we shall see, these assumptions can be replaced by a weaker assumption that the mean atomic density profile does not change. Technically, these assumptions are realized starting with a perturbative approach to solve the Heisenberg equation for the ground-state operators in the zeroth order, and neglecting the influence of the field and spontaneous emission processes. We set therefore

$$g_{\vec{n}}(t) \approx g_{\vec{n}}(0) e^{-iE^g_{\vec{n}} t}, \tag{6}$$

and similarly for $g^\dagger_{\vec{n}}(t)$. The above expressions are then inserted into Eqs. (3) and (4), which then become linear and can be, at least formally, solved under a decorrelation approximation for the product operators. We accomplish it in two steps. First, we solve formally Eq. (4) and express the operators $\vec{e}_{\vec{m}}$, $\vec{e}^\dagger_{\vec{m}}$ in terms of $a_{\vec{k}\mu}$, $a^\dagger_{\vec{k}\mu}$, respectively. Second, we insert the formal solutions into Eq. (3), and perform an average over all quantum fluctuations. This average consists, in particular, in averaging over the initial atomic distribution, which is described by the Bose-Einstein distribution, so that

$$\langle g^\dagger_{\vec{n}}(0) g_{\vec{n}'}(0)\rangle = \delta_{\vec{n}\vec{n}'} N_{\vec{n}} = \delta_{\vec{n}\vec{n}'} \frac{z e^{-\beta E_{\vec{n}}}}{1 - z e^{-\beta E_{\vec{n}}}}, \tag{7}$$

where $\beta = 1/kT$, and z is the fugacity. The decorrelation approximation for the fluctuations of the EM field and the atomic distribution allow us to replace $\langle g^\dagger_{\vec{n}}(0) g_{\vec{n}'}(0) a_{\vec{k}\mu}(t)\rangle$ by $\langle g^\dagger_{\vec{n}}(0) g_{\vec{n}'}(0)\rangle \langle a_{\vec{k}\mu}(t)\rangle$ [29,30].

As a result we obtain two independent and complex conjugated scattering equations for the averaged EM field operators $\langle a_{\vec{k}\mu}\rangle$, and $\langle a^\dagger_{\vec{k}\mu}\rangle$. To avoid the proliferation of notation we omit the quantum average in the following. From now on, the symbols $a_{\vec{k}\mu}$ and $a^\dagger_{\vec{k}\mu}$ will denote the averaged photonic operators.

The scattering equation takes in the time domain the form

$$\dot{a}_{\vec{k}\mu}(t) = -ickA_{\vec{k}\mu}(t) - \sum_{\mu'} \int d\vec{k}' \times \int_0^t dt' \mathscr{K}(t-t';\vec{k},\mu,\vec{k}',\mu') a_{\vec{k}'\mu'}(t'), \tag{8}$$

where the *self-energy kernel* is defined as

$$\mathscr{K}(\tau;\vec{k},\mu,\vec{k}',\mu') = (\vec{\epsilon}_{\vec{k}\mu} \cdot \vec{\epsilon}_{\vec{k}'\mu'}) \rho(k) \rho(k') \mathscr{L}(\tau;\vec{k},\vec{k}'), \tag{9}$$

while the reduced kernel is

$$\mathscr{L}(\tau;\vec{k},\vec{k}') = \sum_{\vec{n},\vec{m}} N_{\vec{n}} \eta_{\vec{n}\vec{m}}(\vec{k}) [\eta_{\vec{n}\vec{m}}(\vec{k}')]^* \times \exp[-i(E^e_{\vec{m}} + \omega_0 - E^g_{\vec{n}})\tau]. \tag{10}$$

It is often more convenient to solve the scattering problem in the Laplace-transformed space defined according to [31]

$$\tilde{o}(s) = \int_0^\infty dt e^{-st} o(t). \tag{11}$$

The reduced kernel now takes the form [32]

$$\tilde{\mathscr{L}}(s;\vec{k},\vec{k}') = \sum_{\vec{n},\vec{m}} N_{\vec{n}} \frac{\eta_{\vec{n}\vec{m}}(\vec{k}) [\eta_{\vec{n}\vec{m}}(\vec{k}')]^*}{s + i(E^e_{\vec{m}} + \omega_0 - E^g_{\vec{n}})}. \tag{12}$$

The physical interpretation of the self-energy kernel is simple. It describes the amplitude for the process of the formation of a wave packet in the excited-state trap potential due to absorbtion of a photon of momentum $\vec{k}'$ and polarization μ' at time t', followed by a free evolution of the wave packet within the time interval $\tau = t - t'$. The free evolution consists primarily in quantum diffusion and drift caused by the momentum of the absorbed photon, and terminates at time t when recombination to the ground electronic state accompanied by emission of a photon of momentum $\vec{k}$ and polarization μ takes place.

As we shall demonstrate in Sec. III, the reduced kernel can be approximated for parameters of interest by

$$\tilde{\mathscr{L}}(s;\vec{k},\vec{k}') \simeq \frac{\sum_{\vec{n},\vec{m}} N_{\vec{n}} \eta_{\vec{n}\vec{m}}(\vec{k}) [\eta_{\vec{n}\vec{m}}(\vec{k}')]^*}{s + i(\omega_0 + k_L^2/2M) + \Gamma}, \tag{13}$$

where k_L denotes the wave number of the incident light, M is the atomic mass, and Γ denotes the effective width of the line. The denominator in the above formula describes a resonance shifted by the photon recoil energy, $k_L^2/2M$, and broadened by Γ. In the idealized model that neglects spontaneous emission events out of the condensate, Γ results from the combined effects of the quantum diffusion and drift of the excited atoms wave packets. In Appendix B we show that if such spontaneous emission events are taken into account, Γ attains an additional contribution of the order of single atom natural linewidth γ.

Using the completeness of the $\vec{m}$ states, the sum over $\vec{m}$ can be performed independent of the shape of the excited-state potential. We obtain

$$\tilde{\mathscr{L}}(s;\vec{k},\vec{k}') = \frac{\sum_{\vec{n}} N_{\vec{n}} \eta_{\vec{n}\vec{n}}(\vec{k} - \vec{k}')}{s + i(\omega_0 + k_L^2/2M) + \Gamma} = \frac{\bar{\rho}(\vec{k} - \vec{k}')}{s + i(\omega_0 + k_L^2/2M) + \Gamma}, \tag{14}$$

where

$$\bar{\rho}(\vec{k})=\int d\vec{R}\rho(\vec{R})e^{-i\vec{k}\cdot\vec{R}} \tag{15}$$

is the *form factor*, or the Fourier transform of the equilibrium density

$$\rho(\vec{R})=\sum_{\vec{n}} N_{\vec{n}}|\langle\vec{R}|\vec{n}\rangle|^2. \tag{16}$$

Therefore, as in the case of scattering of strong light pulses [2], the study of weak light scattering off the interacting condensate can be facilitated by using the self-consistent atomic density profiles (see Sec. IV).

The expression given by Eq. (14) provides the main result of this section, since it implies that the self-energy kernel, and thus all the physics of the scattering process, is fully determined by the atomic density profile in equilibrium. Moreover, as we have shown in paper I, the expression analogous to Eq. (14) is generally valid for class B and class C models that incorporate the effects of short-range atom-atom interactions, provided the mean density in Eq. (16) is calculated under the same assumptions. For instance, for class B models one should include density-dependent shifts of the resonance [12]. For the class C models one could use the density profile constructed in the framework of the self-consistent Bogoliubov-Hartree theory. In numerical calculations to be discussed below we will make use of Eq. (14).

III. THE SELF-ENERGY KERNEL

In this section we demonstrate that in the range of parameters of interest for current experiments the reduced scattering kernel is accurately described by Eq. (14). We shall illustrate this point by using two analytically solvable cases: (a) when the excited-state potential is absolutely flat (the case of a zero potential); and (b) when the excited-state potential is exactly the same as the ground-state harmonic oscillator potential. Both examples will be elaborated for class A models at $T=0$, but the approximations that we use can be equally well applied to class B and C models. Extension to the case $T\neq 0$ is discussed in Appendix C.

A. Zero potential for the excited state

In the case when there is no trapping potential for the excited state, the $|\vec{m}\rangle$ correspond in the spatial representation to a plane-wave state (from now on, where appropriate, $\vec{m}$ should be understood to stand for the center-of-mass momentum for the excited wave packet).

$$\langle\vec{R}|\vec{m}\rangle=\frac{1}{(2\pi)^{3/2}}e^{i\vec{m}\cdot\vec{R}}, \tag{17}$$

and have the corresponding energies

$$E^e_{\vec{m}}=\frac{\vec{m}^2}{2M}=\omega_t\vec{m}^2a^2. \tag{18}$$

The latter relation does not hold for class A* models, in which we treat a and ω_t as independent parameters in order to account phenomenologically for effects of atom-atom interactions [1]. At zero temperature, all atoms are in the condensate, i.e.,

$$N_{\vec{n}}=N\delta_{\vec{n}0}. \tag{19}$$

The relevant Franck-Condon parameter then becomes the Fourier transform of the ground-state wave function, and is given by

$$\eta_{0\vec{m}}(\vec{k})=\left(\frac{2a^2}{\pi}\right)^{3/4}e^{-(\vec{k}-\vec{m})^2a^2}. \tag{20}$$

The reduced kernel Eq. (10) becomes a three-dimensional Gaussian integral with respect to $\vec{m}$, which can be easily performed. We obtain

$$\mathscr{L}(\tau;\vec{k},\vec{k}')=N\frac{1}{(1+i\omega_t\tau/2)^{3/2}}\times\exp\left[-i\omega_0\tau-[k^2+(k')^2]a^2+\frac{(\vec{k}+\vec{k}')^2a^2}{2(1+i\omega_t\tau/2)}\right]. \tag{21}$$

The physical interpretation of the above expression is straightforward. The free propagation of the excited wave packet (20) consists (in the absence of the excited-state potential) in quantum diffusion and drift due to photon recoil. The time-dependent prefactor in Eq. (21) results directly from quantum diffusion effects. The time dependence in the exponent in Eq. (21) accounts for both of the above-mentioned effects. In the regime of parameters that we consider $k\simeq k'\simeq 2\pi/\lambda$, the products $ka\simeq k'a\simeq 8-80$. The kernel (21) contains thus an exponentially small factor $\exp\{-[k^2+(k')^2]a^2\}$, which has to be compensated by the last term in the exponent of Eq. (21) in order to attain non-negligible value. Physically, this means that as the diffusion and drift of the excited wave packet proceeds, the wave packet is moved away from the center of the trap, and the probability of recombination decreases practically to zero. The kernel (21) can be significantly different from zero only for sufficiently short times, such that $\omega_t\tau\ll 1$ [33].

We can therefore perform an expansion in $\omega_t\tau$ in the exponent of (21), and keep only the first- and second-order terms. In doing so we replace the diffusion factor $1/(1+i\omega_t\tau/2)^{3/2}$ by 1. Alternatively, we could represent it in the exponential form as well, but the latter step is not necessary for $ka,k'a\gg 1$ [33]. It would, however, play a role if we should wish to extend the theory to $ka,k'a\simeq 1$.

As a result we obtain the reduced kernel

$$\mathscr{L}(\tau;\vec{k},\vec{k}')=N\exp[-(\vec{k}-\vec{k}')^2a^2/2-\mathscr{P}_2\tau^2-i\omega_0\tau-i\omega_t\tau(\vec{k}+\vec{k}')^2a^2/4], \tag{22}$$

and its Laplace transform

$$\tilde{\mathscr{L}}(s;\vec{k},\vec{k}')=N\exp\left[-\frac{1}{2}(\vec{k}-\vec{k}')^2a^2\right]\frac{\sqrt{\pi}}{2\sqrt{\mathscr{P}_2}}\times\exp\left(\frac{\mathscr{P}_1}{2\sqrt{\mathscr{P}_2}}\right)^2\operatorname{erfc}\left(\frac{\mathscr{P}_1}{2\sqrt{\mathscr{P}_2}}\right), \tag{23}$$

where

$$\mathscr{P}_2=\omega_t^2(\vec{k}+\vec{k}')^2a^2/8\simeq\omega_t^2k_L^2a^2/2, \tag{24}$$

$$\mathscr{P}_1=s+i\omega_0+i\omega_t(\vec{k}+\vec{k}')^2a^2/4\simeq s+i\omega_0+ik_L^2/2M, \tag{25}$$

with $k_L=2\pi/\lambda$, and erfc() denoting the error function [31]. The first exponential factor in Eq. (23) expresses the approximate photon momentum conservation for scattering off a sample of finite size. From Eq. (22) we conclude that the actual decay constant of the kernel is of the order of $\Gamma\sim\sqrt{2\mathscr{P}_2}\simeq\omega_tk_La$. For the idealized model (without spontaneous emission out of condensate) Γ ranges from 300 Hz for a 1-μm trap to 30 Hz for a 10-μm trap (for Cs atoms). In Appendix B we show that spontaneous emission out of the condensate leads to the broadening of the atomic line $\omega_0\rightarrow\omega_0-i\bar{\gamma}$, so that the decay constant of the kernel Γ attains an additional contribution $\bar{\gamma}$ of the order of the natural linewidth γ.

As will be demonstrated in Sec. V, for the calculation of the scattering amplitude one needs only the value of $\tilde{\mathscr{L}}(s;\vec{k},\vec{k}')$ evaluated at $s=-i\omega_L=-ick_L$ (on the energy shell). For most of the values of the detuning $\omega_L-\omega_0$, the argument of the error function in Eq. (23) is large, and the asymptotic expansion

$$\sqrt{\pi}z\exp(z^2)\mathrm{erfc}(z)\simeq1, \tag{26}$$

can be used. At the exact resonance, on the other hand, the kernel remains finite. This suggests the following analytic approximation,

$$\tilde{\mathscr{L}}(s;\vec{k},\vec{k}')\simeq N\exp[-(\vec{k}-\vec{k}')^2a^2/2]\frac{A}{s+i(\omega_0+k_L^2/2M)+\Gamma}. \tag{27}$$

The coefficients A and Γ can be determined from the following two requirements: (i) the asymptotic behavior for large $s+i(\omega_0+k_L^2/2M)$ should be the same for both sides of Eq. (27); and (ii) the values of both expressions should agree at the exact resonance, $s+i(\omega_0+k_L^2/2M)=0$. These requirements give $A=1$ and

$$\Gamma=\Gamma_d=\sqrt{\frac{2}{\pi}}\omega_tk_La, \tag{28}$$

where Γ_d denotes the diffusive linewidth for the model that neglects the effects of spontaneous emission out of the condensate. When those effects are incorporated, and when $\Gamma_d\ll\bar{\gamma}$, the asymptotic expansion of the error function can be used for all detunings, i.e., including resonance. In such a situation

$$\Gamma=\bar{\gamma}. \tag{29}$$

In general, the width Γ is of the order of $\max(\bar{\gamma},\Gamma_d)$, and undergoes Doppler broadening at finite T ($\neq0$).

Direct numerical calculation of the expression Eq. (27) shows that in the regime corresponding to parameters of interest it is very accurate, and produces less than 0.1% relative error for the idealized model, and less than 10^{-4}% for the model including spontaneous emission out of the condensate. This is the major result of this section; it provides a mathematical justification for the expression Eq. (14), which was obtained only heuristically in Sec. II.

B. The same harmonic oscillator potential for the excited state as for the ground state

The above considerations can be generalized to the case of other trap potentials for the excited state. In particular, we consider in this subsection the case where the excited-state potential is harmonic and is the same as the ground-state trapping potential. The indices $\vec{m}$ become (m_x,m_y,m_z), $|\vec{m}\rangle$ are the corresponding eigenstates for the harmonic oscillator, and

$$E^e_{\vec{m}}=\omega_t(m_x+m_y+m_z). \tag{30}$$

The reduced kernel at $T=0$ in this case becomes

$$\mathscr{L}(\tau;\vec{k},\vec{k}')=e^{-i\omega_0\tau}\sum_{\vec{m}}e^{-iE^e_{\vec{m}}\tau}\langle0|e^{-i\vec{k}\cdot\vec{R}}|\vec{m}\rangle\langle\vec{m}|e^{i\vec{k}'\cdot\vec{R}}|0\rangle. \tag{31}$$

Observing that

$$\langle m_x|e^{ik_xR_x}|0_x\rangle=\exp\left[-\frac{1}{2}k_x^2a^2\right]\frac{(ik_xa)^{m_x}}{\sqrt{m_x!}}, \tag{32}$$

we can perform the sum over m_x, m_y, and m_z in Eq. (31) independently. The result is

$$\mathscr{L}(\tau;\vec{k},\vec{k}')=\exp\{-i\omega_0\tau-[k^2+(k')^2]a^2/2+\vec{k}\cdot\vec{k}'a^2e^{-i\omega_t\tau}\}. \tag{33}$$

The expression (33) is similar to (21), but it differs in one important aspect. The excited wave packets do not diffuse and spread as before [35], but rather oscillate coherently in the harmonic well. This means that the small exponential factor $\exp\{-[k^2+(k')^2]a^2/2\}$ can be compensated by the last term in the exponent of Eq. (33) at $\tau\simeq0,\pi/\omega_t,2\pi/\omega_t,\ldots$. Physically, this means that whenever the wave packet returns to the origin, the approximate momentum conservation can be realized. For even returns, the scattering prefers the forward direction, whereas for odd returns it prefers the backward direction. This is very similar to the phenomena of revivals and collapses often discussed in the Jaynes-Cummings model [36]. In principle, one can account for multiple returns by calculating the Laplace transform of $\mathscr{L}(\tau;\vec{k},\vec{k}')$ with the help of saddle-point techniques [37]. Here, however, we will for convenience assume that the probing of the system by weak light has a finite duration τ_d, such that $\omega_t\tau_d\ll1$, i.e., $\tau_d\ll0.1$ s. In this case we can neglect the effects of multiple returns in Eq. (33), and expand the exponent in $\omega_t\tau$, in the same manner as we did in the previous subsection for the case of a zero trapping potential in the excited states. Note, that for weak light pulses of the duration $\tau_d\simeq0.1$ s, one can consider the long time limit of

the scattering process, since τ_d is still much larger than all other relevant time scales (including $1/\Gamma$).

With the above approximations, the Laplace transform of the kernel is again given by the expression (23), where now

$$\mathscr{P}_2 = \omega_t^2 \vec{k}\cdot\vec{k}' a^2/2 \simeq \omega_t^2 k_L^2 a^2/2, \tag{34}$$

$$\mathscr{P}_1 = s + i\omega_0 + i\omega_t \vec{k}\cdot\vec{k}' a^2 \simeq s + i\omega_0 + ik_L^2/2M. \tag{35}$$

Thus, the self-energy kernel can also be approximated by exactly the same formula given by Eq. (27). In Appendix C we generalize this result to the case of a finite temperature $T \neq 0$.

IV. ATOMIC DENSITY PROFILES

The results of Sec. II established the relations (14) and (15) between the self-energy kernel and the atomic density profile. Before we turn to a further discussion of the scattering problem, we thus need to specify the atomic density profiles.

For the class A models we use the density profiles obtained from the Bose-Einstein distribution (BED) for noninteracting atoms according to Eq. (16). In particular, for $T=0$, the density distribution is

$$\rho(\vec{R}) = \frac{N}{(2\pi a^2)^{3/2}} \exp(-R^2/2a^2). \tag{36}$$

As we argued in paper I and Ref. [12], by treating a as a parameter independent of ω_t and M, we can account phenomenologically for effects of the atom-atom interactions for class A* models.

At high temperatures, the BED can be replaced by the Boltzmann distribution and the effects of atomic collisions can be neglected. The density in this limit is again Gaussian,

$$\rho(\vec{R}) = \frac{N}{[2\pi a^2(\beta)]^{3/2}} \exp[-R^2/2a^2(\beta)], \tag{37}$$

with a temperature-dependent width

$$a^2(\beta) = a^2 \coth(\beta\omega_t/2) \simeq 2a^2/\beta\omega_t. \tag{38}$$

The description of the atomic density profile at $T=0$ for a weakly interacting gas is much more difficult, and becomes even more complex at low, but finite temperatures. In order to find the density profile at thermal equilibrium, one has to add to the Hamiltonian (1) a term [1] describing the ground-ground atomic interactions. This term is usually written in the *shape-independent approximation* [38], and has the form

$$\mathscr{H}_{gg} = \frac{b_{gg}}{2}\int d\vec{R}\,\Psi_g^\dagger(\vec{R})\Psi_g^\dagger(\vec{R})\Psi_g(\vec{R})\Psi_g(\vec{R}), \tag{39}$$

where

$$b_{gg} = 4\pi a_{sc}/M, \tag{40}$$

and a_{sc} denotes the scattering length for the ground-ground scattering. In the above formula $\Psi_g(\vec{R})[\Psi_g^\dagger(\vec{R})]$ is the atomic annihilation (creation) field operator. Formally, such a form of the atom-atom interaction Hamiltonian can be derived in the low-energy limit by using the so-called, *T matrix* or *ladder* approximation in the calculations of the single-particle Green's functions using standard many-body techniques [39–41].

In the mean-field Bogoliubov-Hartree approach [23,39] the c-number wave function $\Psi_g(\vec{R})$ of the condensate at $T=0$ is a minimum of the energy functional (see also paper I),

$$E\int d\vec{R}\Psi_g^*(\vec{R})\Psi_g(\vec{R}) = \int d\vec{R}\Psi_g^*(\vec{R})\left(-\frac{\nabla^2}{2M} + \frac{1}{2}M\omega_t R^2\right)\Psi_g(\vec{R}) + \frac{b_{gg}}{2}\int d\vec{R}\Psi_g^*(\vec{R})\Psi_g^*(\vec{R})\Psi_g(\vec{R})\Psi_g(\vec{R}), \tag{41}$$

with the normalization constraint $\int d\vec{R}|\Psi(\vec{R})|^2 = N$. The condensate wave function then fulfills the following nonlinear Schrödinger equation (NLSE):

$$\left[-\frac{\nabla^2}{2M} + \frac{1}{2}M\omega_t R^2 + b_{gg}\rho(\vec{R})\right]\Psi_g(\vec{R}) = E\Psi_g(\vec{R}). \tag{42}$$

For very large N an approximate solution of this NLSE is found to be (by neglecting the kinetic energy term [42])

$$\rho(\vec{R}) = \Psi_g^*(\vec{R})\Psi_g(\vec{R}) \simeq \frac{15N}{8\pi R_0^5}(R_0^2 - R^2), \tag{43}$$

for $R \leqslant R_0$, and zero otherwise. The size of the condensate within this approximation is given by

$$R_0 = a(60Na_{sc}/a)^{1/5}. \tag{44}$$

The above solution evidently is not correct for $R \to R_0$. In general, one then has to rely on numerical solutions to Eq. (42).

Recently Edwards and Burnett [24] have studied the numerical solutions of this equation. Utilizing the spherical symmetry of the condensate, Eq. (42) can be transformed into a differential equation involving the radial coordinate R only. The asymptotic behavior ($R \to \infty$) and the boundary conditions ($R=0$) were studied analytically and enforced during the integration procedure. For a given set of parameters a, N, and b_{gg}, a solution that satisfies both boundary conditions ($R=0,\infty$) was obtained using a Runge-Kutta method. In practice, this is achieved by specifying the value of the radial wave function, and its first-order derivative at $R=0$. The equation for the radial wave function was integrated outwards to sufficiently large R, and then compared to the known asymptotic solution. A solution that has the correct asymptotic behavior is obtained by varying the first-order derivative of the radial wave function at $R=0$. However, the solution thus obtained is not necessarily correctly normalized. Edwards and Burnett observed that the nonlinear radial Schrödinger equation has the property that a normalized solution can be obtained from any solution through a suitable scaling transformation. This normalized solution, however, corresponds to a condensate with a number of at-

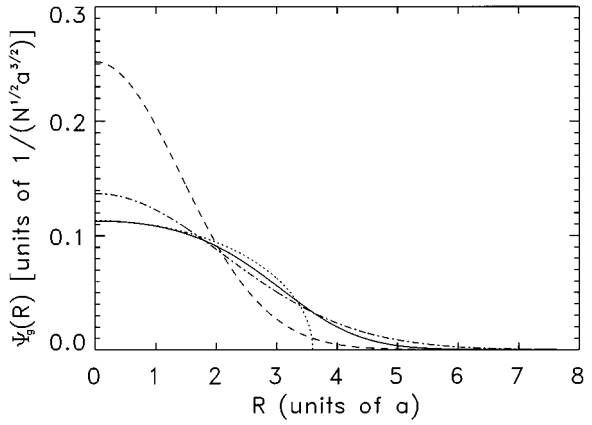

FIG. 1. Comparison of various approximations to the condensate wave function. The solid line denotes the numerical solution of the nonlinear Schrödinger equation (42), and the dotted line denotes the approximate solution given by Eq. (43). The dot-dashed line is a Gaussian with an effective width 1.5 times larger than that of the noninteracting Gaussian ground state represented by the dashed line. The coupling strength in dimensionless scaled units is $N(a_{sc}/a)=10$.

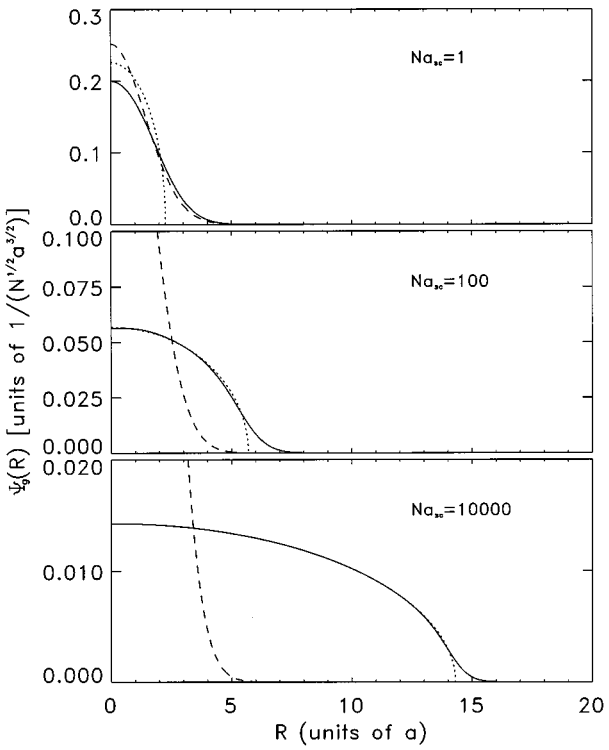

FIG. 2. The lowest eigenvalue solutions of Eq. (42) for three values of the coupling strength Na_{sc} (as listed in the figure) compared with the corresponding approximate solutions given by Eq. (43). The solid line denotes the exact numerical solution and the dotted line denotes the approximate solution given by Eq. (43). The dashed line serves as a reference, and is a single atom Gaussian ground state, which also corresponds to the noninteracting condensate.

oms N that cannot be specified *a priori.* Their scheme of solution of Eq. (42) is therefore not very suitable for our purpose, as we have to compare light-scattering properties of condensates with a *given* number of atoms N. We have therefore developed an alternative scheme for the numerical solution of Eq. (42) [25].

Our scheme is an iterative one. Within each step, we take $\rho(R)$ as given, so that Eq. (42) becomes a standard linear Schrödinger equation. We solve the eigenproblem (i.e., find the eigenvalues and normalized eigenvectors) for this linear equation using a standard matching method coupled with the Pruefer transformation [26]. To find the lowest-energy solution (the ground state) of Eq. (42), we update $\rho(R)=|\Psi_g^{\rm new}(\vec{R})|^2$ by a weighted average of the newly computed lowest eigenvector $\Psi_g^{\rm eigen}(\vec{R})$ and the previous wave function $\Psi_g^{\rm old}(\vec{R})$[used for computing $\rho(R)$]

$$\Psi_g^{\rm new}(\vec{R})\propto(1-\eta_{\rm mix})\Psi_g^{\rm old}(\vec{R})+\eta_{\rm mix}\Psi_g^{\rm eigen}(\vec{R}), \quad (45)$$

where we use the sign "$\propto$" instead of "$=$" since the right-hand side has yet to be correctly normalized. In the above $\eta_{\rm mix}\in(0,1)$ is a mixing parameter. In general the convergence of our method strongly depends on $\eta_{\rm mix}$, and on the parameter Nb_{gg}. The detailed analysis, as well as the results for the collective excited states of the condensate [higher eigenvalues and eigenvectors of Eq. (42)] will be presented elsewhere [25]. The iteration proceeds until both absolute and relative convergence criteria are satisfied. As an added bonus, we find that our method basically converges irrespective of the coupling strength Nb_{gg} (which effectively determines the strength of the interaction or the nonlinearity) if $\eta_{\rm mix}$ is adjusted appropriately.

In Fig. 1 we present a comparison of various approximations to the condensate wave function used in computing the density profile $\rho(R)$. The dashed line denotes the noninteracting (Gaussian) ground state of the harmonic oscillator potential, which serves as the reference, and the solid line denotes the numerical solution (the lowest-energy eigenstate) of the nonlinear Schrödinger equation (42), while the dotted line denotes the approximate solution given by Eq. (43). The dot-dashed line is again a Gaussian but with an effective width 1.5 times larger than that of the noninteracting ground state (the dashed line). The Gaussian with the effective width matches the numerical solution (solid line) quite well. Obviously, since the physical observables are related directly to the density profile, using the Gaussian with the effective width for the class A^* models is a very good approximation. In the calculation we have used a coupling strength $N(a_{sc}/a)=10$. For a 10-μm trap, this corresponds to all possible pairs of parameters (N,a_{sc}), such as, $(10^7,0.1$ Å), $(10^6,1$ Å), $(10^5,10$ Å), . . . , as long as their product remains the same.

In Fig. 2, we plot the lowest eigenvalue solutions of Eq. (42) for three values of the coupling strength Na_{sc} (as listed in the figure) compared with their corresponding approximate solutions as given by Eq. (43). For a condensate with a given N, as the parameter a_{sc} increases the shape of the condensate function changes smoothly from a Gaussian (characteristic for noninteracting atoms) to parabolic one as given by Eq. (43) (characteristic for an interacting gas), and the approximation given by Eq. (43) becomes better and better.

V. ON-SHELL APPROXIMATION

In this section we turn back to a discussion of the solutions of the scattering equation: Eq. (8). In the Laplace-transformed form it reads

$$(s+ick)\tilde{a}_{\vec{k}\mu}(s) = a_{\vec{k}\mu}(0) - \sum_{\mu'} \int d\vec{k}'\, \tilde{\mathscr{K}}(s;\vec{k},\mu,\vec{k}',\mu')\tilde{a}_{\vec{k}'\mu'}(s), \quad (46)$$

where

$$a_{\vec{k}\mu}(0) = \alpha\,\delta(\vec{k}-\vec{k}_L)\,\delta_{\mu\mu_L}, \quad (47)$$

corresponds to the incident coherent laser field of wave vector $\vec{k}_L$, polarization $\vec{\epsilon}_{k_L\mu_L}$, and amplitude α. The on-shell approximation to the scattering problem is formulated as follows.

First, we divide the total field into incident and scattered parts,

$$\tilde{a}_{\vec{k}\mu}(s) = \frac{1}{s+i\omega_L}\alpha\,\delta(\vec{k}-\vec{k}_L)\,\delta_{\mu\mu_L} + \tilde{a}^{\rm sc}_{\vec{k}\mu}(s), \quad (48)$$

and obtain an equation for the scattered field

$$\tilde{a}^{\rm sc}_{\vec{k}\mu}(s) = -\frac{\alpha}{(s+i\omega_L)(s+ick)}\tilde{\mathscr{K}}(s;\vec{k},\mu,\vec{k}_L,\mu_L) - \sum_{\mu'} \int d\vec{k}'\, \tilde{\mathscr{K}}(s;\vec{k},\mu,\vec{k}',\mu')\frac{\tilde{a}^{\rm sc}_{\vec{k}'\mu'}(s)}{s+ick}. \quad (49)$$

In the limit $t\to\infty$ (or practically, $t\gg 1/\Gamma$) the incident field has enough time to penetrate the system and *a long time coherent response* will build up. Therefore we postulate that asymptotically the scattered field behaves as

$$a^{\rm sc}_{\vec{k}\mu}(t) \sim \alpha B(\vec{k},\mu)\,\delta(ck-\omega_L)e^{-i\omega_L t}, \quad (50)$$

and its Laplace transform,

$$\tilde{a}^{\rm sc}_{\vec{k}\mu}(s) \sim \frac{\alpha}{s+i\omega_L}B(\vec{k},\mu)\,\delta(ck-\omega_L), \quad (51)$$

where $B(\vec{k},\mu)$ is the scattering amplitude. Thus in this approximation as $t\to\infty$ only coherent *elastic* scattering is possible.

Inserting the above expressions into Eq. (49), transforming back to the time domain, and taking the limit $t\to\infty$, we conclude that the scattering amplitude in this on-shell approximation [18] as assumed by Eq. (50) satisfies

$$B(\vec{k},\mu) = -2\pi\tilde{\mathscr{K}}(-i\omega_L;\vec{k},\mu,\vec{k}_L,\mu_L) - 2\pi\frac{k_L^2}{c}\sum_{\mu'}\int d\Omega_{\vec{k}'} \times \tilde{\mathscr{K}}(-i\omega_L;\vec{k},\mu,\vec{k}',\mu')B(\vec{k}',\mu'), \quad (52)$$

where $|\vec{k}|=|\vec{k}'|=|\vec{k}_L|=\omega_L/c$. In deriving the above equation we have used the identity

$$\lim_{t\to\infty}\frac{1}{2\pi i}\int ds e^{st}\frac{\tilde{f}(s)}{(s+i\omega_L)(s+ick)} = \lim_{t\to\infty}\left[\frac{\tilde{f}(-i\omega_L)e^{-i\omega_L t}-f(-ick)e^{-ickt}}{i(ck-\omega_L)}\right] = 2\pi\tilde{f}(-i\omega_L)e^{-i\omega_L t}\delta(ck-\omega_L), \quad (53)$$

which holds for an arbitrary function $\tilde{f}(s)$ provided it does not have any singularities to the right of or on the imaginary axis in the complex s plane, so that $\lim_{t\to\infty}f(t)=0$. One might also try to solve Eq. (52) using the Born approximation, i.e., neglecting the second, self-energy term on the right-hand side. Such attempts are reasonable in the low-density limit [13], but fail miserably in the regime of parameters that we consider. This is partially due to the large optical thickness of the condensate, since after an incident photon is absorbed, it takes on average very many rescattering events before it escapes the condensate. Self-energy terms are extremely important close to resonance and one must fully account for them. One may also try to solve Eq. (52) numerically. To accomplish this we discretized the solid angle and solved the resulting finite set of linear equations on a grid. However, in the regime of parameters of interest, the dimensions of the resulting finite difference equations are quite large, and its numerical solutions become quite difficult and expensive to obtain. Consequently, they have only been used as a guidance for developing approximate analytic solutions.

One can construct an approximate analytic solution for Eq. (52), if one (i) substitutes the product $\rho(k)\rho(k')$ in $\tilde{\mathscr{K}}$ by $|\rho(k_L)|^2$, and (ii) neglects the dependence of $\tilde{\mathscr{K}}$ on the polarization product $\vec{\epsilon}_{\vec{k}\mu}\cdot\vec{\epsilon}_{\vec{k}'\mu'}$. The first of these approximations is obviously very accurate, since $\rho(k)$ is an extremely slowly varying function of k in the optical regime. The second approximation is also quite accurate, since the scattering occurs mainly in the forward direction and the scattered photons have polarizations that are approximately perpendicular to $\vec{k}_L$, and do not couple to the other polarization component strongly.

After performing the two above-mentioned approximations, $B(\vec{k},\mu)$ can be expanded in spherical harmonics. For $\vec{k}=k_L(\sin\theta\cos\phi,\sin\theta\sin\phi,\cos\theta)$, $\vec{k}_L=k_L(0,0,1)$, and $\vec{\epsilon}_{\mu_L}=(1,0,0)$, the expansion is

$$B(\vec{k},\mu) = \sum_{l=0}^{\infty} B_l(k_L)P_l[\cos(\theta)](2l+1)/4\pi, \quad (54)$$

where $P_l(x)$ are Legendre polynomials. Since spherical harmonics are now eigenvectors of the scattering kernel on the energy shell, the coefficients $B_l(k_L)$ can be directly obtained as

$$B_l(k_L) = -\frac{\gamma_L^l}{[\Gamma+\gamma_L^l-i(\omega_L-\omega_0-k_L^2/2M)]}\frac{c}{k_L^2}, \quad (55)$$

where

$$\gamma_L^l = 12\pi\gamma\mathcal{O}_l, \tag{56}$$

with

$$\mathcal{O}_l = \int_0^\infty R^2 dR \rho(R) j_l^2(k_L R). \tag{57}$$

Here $j_l()$ denotes a spherical Bessel function. Comparison of the above expressions with the numerical solution of Eq. (52) shows that the approximate solution describes the line shape very well, although it underestimates the overall cross section typically by 10–20 %. The above expressions can be further elaborated analytically, after specifying the atomic density profile. For a Gaussian profile as given by Eq. (36), for instance, we obtain

$$\gamma_L^l = N\gamma 3\sqrt{2\pi} e^{-k_L^2 a^2} I_{l+1/2}(k_L^2 a^2)/(2k_L a), \tag{58}$$

where $I_l()$ denotes a modified Bessel function.

The quantities of interest are (i) the total number of elastically scattered photons of frequency ω_L, per unit time and normalized to the total number of photons incident upon the area πa^2 (normalized cross section), given by (see Appendix A)

$$\sigma_{\rm scatt}(\omega_L) = \frac{4\pi}{(k_L a)^2}\left(\frac{k_L^2}{c}\right)^2 \sum_\mu \int d\Omega_{\vec{k}} |B(\vec{k},\mu)|^2; \tag{59}$$

and (ii) the total cross section $\sigma_{\rm tot}(\omega_L)$, being the sum of $\sigma_{\rm scatt}(\omega_L)$ and the *absorption* cross section $\sigma_{\rm abs}(\omega_L)$; $\sigma_{\rm tot}(\omega_L)$ is determined from the optical theorem ([18], see also Appendix A).

Using the partial wave expansion, the total scattering cross section becomes

$$\begin{aligned}\sigma_{\rm scatt} &= \frac{1}{(k_L a)^2}\left(\frac{k_L^2}{c}\right)^2 \sum_{l=0}^\infty (2l+1)|B_l(k_L)|^2 \\ &= \frac{1}{(k_L a)^2}\sum_{l=0}^\infty (2l+1)\frac{(\gamma_L^l)^2}{(\gamma_{\rm eff}^l)^2 + (\omega_L - \omega_0 - k_L^2/2M)^2},\end{aligned} \tag{60}$$

i.e., the sum of Lorentzians (55), characterized by the width $\gamma_{\rm eff}^l = \Gamma + \gamma_L^l$, and the corresponding differential cross section only depends on the polar angle θ, and is given by

$$d\sigma_{\rm scatt}(\theta,\omega_L) = \frac{1}{2(k_L a)^2}\left|\sum_{l=0}^\infty (2l+1)\frac{\gamma_L^l}{[\gamma_{\rm eff}^l - i(\omega_L - \omega_0 - k_L^2/2M)]} P_l[\cos(\theta)]\right|^2 \sin(\theta) d\theta. \tag{61}$$

A similar expression holds for $\sigma_{\rm tot}$, i.e.,

$$\begin{aligned}\sigma_{\rm tot}(\omega_L) &= -\frac{8\pi}{(k_L a)^2}\frac{k_L^2}{c}\,{\rm Re}[B(\vec{k}_L,\mu_L)] \\ &= \frac{2}{(k_L a)^2}\sum_{l=0}^\infty (2l+1)\frac{\gamma_L^l \gamma_{\rm eff}^l}{(\gamma_{\rm eff}^l)^2 + (\omega_L - \omega_0 - k_L^2/2M)^2}.\end{aligned} \tag{62}$$

We note that in general $\sigma_{\rm tot} \geqslant 2\sigma_{\rm scatt}$, i.e., there are always more absorption events than scattering events. In the idealized model for the scattering kernel with the very small Γ, we have $\sigma_{\rm tot} \simeq 2\sigma_{\rm scatt}$. For the parameters we are using, the dominant contribution to the sums in Eqs. (61) and (62) comes from l values with $\gamma_L^l \gg \Gamma$, therefore the absorption and the scattering cross sections are approximately the same, i.e., $\sigma_{\rm abs} \approx \sigma_{\rm scatt}$.

We analyze the result given by Eq. (60) with the help of the formula Eq. (58). Note that the Gaussian function used to derive Eq. (58) describes the density profile for class A models with a harmonic potential, class A* models, and all classes of models in the high-temperature limit. We can thus use Eq. (58) in all these cases provided the value of a is appropriately adjusted.

For $l \ll k_L^2 a^2$, all γ_L^l's are roughly equal to $\gamma_{\rm eff} \approx 3N\gamma/(2k_L^2 a^2)$ [11]. One might think that if only low angular momentum harmonics contribute to scattering, the cross section would be a sum of Lorentzians with approximately the same width; i.e., it would itself be a Lorentzian. However, the γ_L^l's decrease quite significantly with increasing l. In fact, the contribution from higher l's is also important. As a result, the line shape becomes non-Lorentzian, and exhibits a very narrow spike close to resonance. This narrow feature in the spectrum is an analog of the coherent Dicke narrowing [43]. The lower bound for the width of this spike is determined by the rate Γ, which in the model that accounts for spontaneous emission out of the condensate is of the order of the sum of the natural linewidth and diffusive broadening Γ_d. It is worth noticing that even close to resonance the angular distribution of the scattered light has a width of the order $1/(k_L a)$. We shall discuss the line shapes in detail in Sec. VII.

We summarize this section by stressing once more that the on-shell approximation has many appealing properties: it allows for an accurate analytic solution of the scattering problem, and for a direct analysis of the cross sections in terms of partial waves. It also provides a representation of the cross sections in the form of a sum of Lorentzians with decreasing width. The latter representation allows us to recover Javanainen's result [11], in the limit in which the contribution from the lower partial waves is dominant. On the other hand, the on-shell approximation has two major drawbacks: its validity range is not well established, and, according to Eq.

(50), as $t\to\infty$ it treats each of the multiple scattering events as elastic [to see that multiple scattering occurs one may consider an iterative solution of Eqs. (8) or (46)]. The latter statement implies that this approximation presumably cannot be used for very dense systems for which *off-shell* propagation between the successive scattering events might play a significant role. In Sec. VI we present another solution of the scattering problem which employs Glauber's GDT, which should account much more accurately for the off-shell propagation effects.

VI. GENERALIZED DIFFRACTION THEORY

In order to apply the GDT [19] we perform the same approximations to the self-energy kernel as in Sec. V, i.e., replace $\rho(k)\rho(k')$ by $|\rho(k_L)|^2$, and neglect the polarization dependence in Eq. (14). In the long time limit, we may also replace $\tilde{\mathscr{K}}(s;\vec{k},\mu,\vec{k}',\mu')$ in Eq. (46) by $\tilde{\mathscr{K}}(-i\omega_L;\vec{k},\mu,\vec{k}',\mu')$ [45]. Equation (46) may now be conveniently transformed to the spatial representation. To achieve this we multiply the left-hand side by $s-ick$, the right-hand side by $-2ick\simeq s-ick$, and introduce the scalar field

$$\mathscr{E}(\vec{R})\propto\int d\vec{k}\rho(k)e^{i\vec{k}\cdot\vec{R}}a_{\vec{k}\mu}. \tag{63}$$

Within the framework of the approximations used, this scalar field is proportional to a component of the electric field propagating in the direction close to $\vec{k}_L$, with polarization close to $\vec{\epsilon}_{\mu_L}$. In the time domain this field fulfills the wave equation,

$$\left[-\frac{\partial^2}{\partial t^2}+c^2\nabla^2\right]\mathscr{E}(\vec{R})=2\omega_L V(\vec{R})\mathscr{E}(\vec{R}), \tag{64}$$

where the complex potential [related to the spatial Fourier transform of the scattering kernel as given by Eq. (14)] is

$$V(\vec{R})=\frac{(2\pi)^3|\rho(k_L)|^2}{\Delta+i\Gamma}\rho(\vec{R}), \tag{65}$$

with $\Delta=\omega_L-(\omega_0+k_L^2/2M)$ being the detuning from the recoil shifted resonance. Physically, the imaginary part of this potential describes the absorption processes. In the idealized model, these processes lead to the excitation of atomic wave packets which then diffuse, and drift away from the trap, without having any possibility of returning their energy back to the field. In the more realistic model of Appendix B the absorbed energy is also dissipated in the processes of spontaneous emission out of the condensate, which subsequently contributes to the incoherently scattered photons.

According to the GDT, when the incident wave propagates in the z direction one seeks a solution of Eq. (64) in the form

$$\mathscr{E}(\vec{R})=e^{-i\omega_L t+ik_L z}\psi(\vec{R}), \tag{66}$$

where $\psi(\vec{R})$ is a slowly varying function of $\vec{R}$. Neglecting its second-order derivatives (in the same way as the slowly varying envelope approximation normally used in studying propagational problems), we obtain

$$\frac{\partial\psi(\vec{R})}{\partial z}=-i\frac{1}{c}V(\vec{R})\psi(\vec{R}), \tag{67}$$

and hence

$$\psi(x,y,z)=e^{-(i/c)\int_{-\infty}^{z}V(x,y,z')dz'}. \tag{68}$$

Let us denote by $\vec{p}$ (the impact parameter) a vector in the (x,y) plane, and by $\hat{z}$ a unit vector in the direction of propagation of the incident wave. It is also convenient to introduce the quantity

$$\chi(\vec{p})=-\frac{1}{c}\int_{-\infty}^{\infty}V(\vec{p}+\hat{z}z)dz. \tag{69}$$

The scattering amplitude can then be expressed as [19]

$$f(\vec{k},,\vec{k}_L)=\frac{k_L}{2\pi i}\int d\vec{p}e^{i(\vec{k}_L-\vec{k})\cdot\vec{p}}[e^{i\chi(\vec{p})}-1]. \tag{70}$$

The scattering and total cross sections are

$$\sigma_{\rm scatt}=\int d\vec{p}|e^{i\chi(\vec{p})}-1|^2, \tag{71}$$

and

$$\sigma_{\rm tot}=\frac{4\pi}{k_L}\,{\rm Im}[f(\vec{k}_L,\vec{k}_L)]$$
$$=2\ {\rm Re}\left\{\int d\vec{p}[1-e^{i\chi(\vec{p})}]\right\}. \tag{72}$$

The above expressions can be further elaborated analytically. For instance, for the case of a Gaussian density profile (see, for instance, [20]) as given by Eq. (36), we get

$$\chi(\vec{p})=-\frac{3N\gamma}{2(k_L a)^2}\frac{e^{-p^2/2a^2}}{\Delta+i\Gamma}, \tag{73}$$

and the cross sections (in units of πa^2) can be expressed in terms of the exponential integral function [31]

$$\sigma_{\rm tot}=4\ {\rm Re}[E_1(\xi_{\rm tot})+\ln(\xi_{\rm tot})+\gamma_E], \tag{74}$$

$$\sigma_{\rm abs}=2[E_1(\xi_{\rm abs})+\ln(\xi_{\rm abs})+\gamma_E], \tag{75}$$

$$\sigma_{\rm scatt}=\sigma_{\rm tot}-\sigma_{\rm abs}, \tag{76}$$

where $E_1()$ is the exponential integral function, $\gamma_E=0.577\,215\,664\,9\ldots$ is Euler's constant, and

$$\xi_{\rm tot}=i\frac{3N\gamma}{2(k_L a)^2}\frac{1}{\Delta+i\Gamma}, \tag{77}$$

$$\xi_{\rm abs}=\frac{3N\gamma}{2(k_L a)^2}\frac{2\Gamma}{\Delta^2+\Gamma^2}. \tag{78}$$

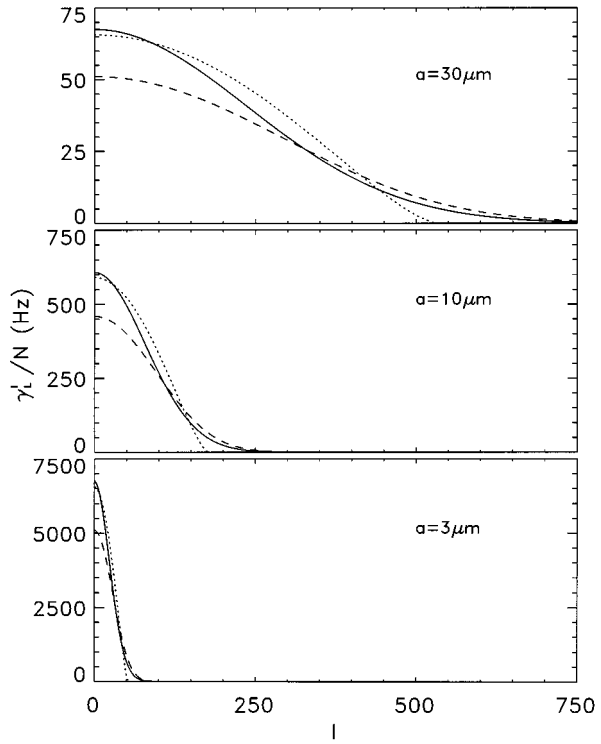

FIG. 3. The partial Lorentzian width γ_L^l as a function of l for three different values of the trap size: $a=30$, 10, and $3\,\mu$m, respectively. The solid lines represent the results given by Eq. (58) for an ideal noninteracting gas, while the dashed (dotted) lines (overlay each other as the approximation is very good in this case) represent results obtained for density profiles obtained from the numerical solutions of the NLSE (42) [approximate solutions of the NLSE given by Eq. (43)] with a coupling strength $Na_{sc}=1$.

Similarly, analytic expressions in terms of hypergeometric functions can be obtained for the density profile of Eq. (43) [33]. In general, within the GDT, we can also use numerical integration techniques to evaluate the cross sections and angular distributions of the scattered field for density profiles such as those obtained from the solutions of the nonlinear Schrödinger equation Eq. (42) [33].

We can also consider the angular distributions within the GDT. As shown by Glauber in Ref. [19], on the energy shell for elastic scattering, after performing the angular integrals one should use

$$\frac{1}{2\pi}\int e^{i(\vec{k}_L-\vec{k})\cdot\vec{p}}d\vec{p}\{\cdots\}=\int_0^\infty J_0\left(2kp\,\sin\frac{\theta}{2}\right)pdp\{\cdots\}, \tag{79}$$

and consequently the scattering amplitude takes the form

$$f(\theta)=-ik_L\int_0^\infty J_0\left(2kp\,\sin\frac{\theta}{2}\right)[e^{i\chi(\vec{p})}-1]pdp. \tag{80}$$

The angular distribution for the elastic scattering is thus

$$\frac{d\sigma_{\rm scatt}(\theta)}{d\theta}=2\pi|f(\theta)|^2\,\sin\theta. \tag{81}$$

Apart from its simplicity, which allows us to obtain many analytic results, GDT has another appealing property: the conditions for its validity regime are well established, and are given by

$$\frac{|V|_{\max}}{\omega_L}\ll 1, \tag{82}$$

where $|V|_{\max}$ denotes the maximal value of the complex potential given by Eq. (65), and

$$k_L a\gg 1. \tag{83}$$

The product of the parameters of Eqs. (82) and (83) may be arbitrarily large, and thus in this sense the GDT is capable of describing strongly nonperturbative effects. The second of the above conditions is fulfilled in the regime of parameters we consider $[a=(1\text{–}20)\lambda]$. The first condition physically means that the GDT in the manner of the eikonal approximation describes high-energy scattering, when the energy of incoming photons is significantly larger than that of the corresponding potential barrier. Obviously, in such situations, scattering, although highly nonperturbative, occurs mainly in the forward direction. In the polariton picture discussed in Refs. [9,10] this corresponds to the case where the photon frequency lies outside the gap, which is formed in the excitation spectrum, or to the case of finite trap size when the line shape is broadened so much that the effects of the gap cease to exist. We examine in more detail below the condition of Eq. (82) for the case of class A models, class A* models with a Gaussian density profile, and a phenomenologically adjusted a, and for the class C models.

The condition (82) for the case of a Gaussian density profile may be written as

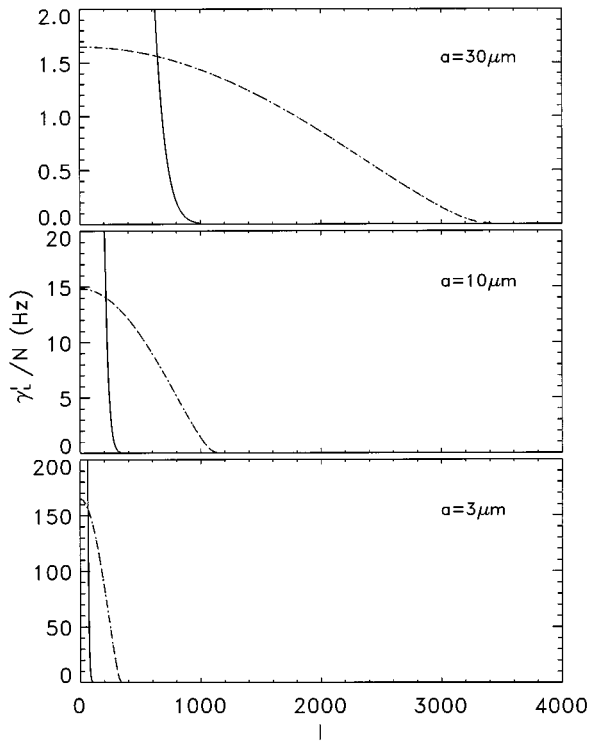

FIG. 4. Same as Fig. 3 except for $Na_{sc}=10\,000$. Dotted lines can hardly be distinguished from the solid ones.

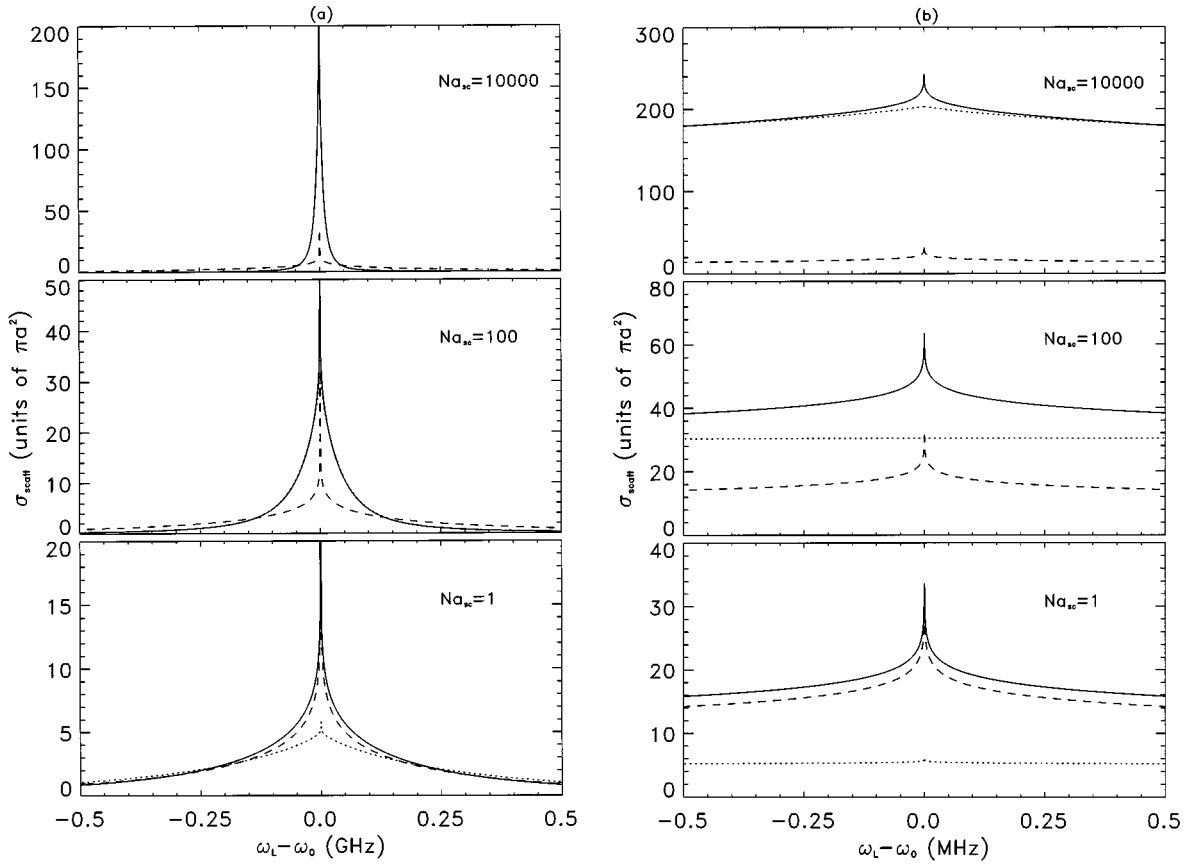

FIG. 5. Typical results for the scattering cross sections obtained from the on-shell approximation for three different values of the interaction strength $Na_{sc}=10\,000, 100,$ and 1 respectively, and $\Gamma=ka\omega_t=31.4$ Hz. The solid lines represent the results obtained from the density profile of the numerical solutions of the nonlinear Schrödinger equation (42). The dotted line represents the results obtained for the approximate density profiles given by Eq. (43). The dashed lines serve as a reference and are obtained for noninteracting gases with the Gaussian density profile given by Eq. (36); (a) large-scale plot of the scattering cross section; (b) enlargement of the central region of (a). [Note: change of units in (b) from GHz to MHz.]

$$\frac{3}{\sqrt{2\pi}}\frac{N}{(k_L a)^3}\frac{\gamma}{\max(|\Delta|,\Gamma)}<1. \tag{84}$$

Similarly for the class C model with the density profile of Eq. (43), the condition becomes

$$\frac{45}{4}\frac{N}{(k_L R_0)^3}\frac{\gamma}{\max(|\Delta|,\Gamma)}<1. \tag{85}$$

We obtain then the following ranges of applicability of our theory:

(i) For $T=0$, $N=10^7$, $a=10$ μm our results for class A models are valid for

$$|\Delta|>20\gamma, \tag{86}$$

i.e., on a scale of tens of MHz. For the class C models with the density profile given by Eq. (43), a scattering length $a_{sc}=20$ Å, and the rest of the parameters the same, the validity condition becomes

$$\max(|\Delta|,\Gamma)>0.2\gamma. \tag{87}$$

Since for realistic models that take into account spontaneous emission out of the condensate, Γ is of the order of γ, we conclude that the inequality Eq. (87) is always fulfilled, and *the theory for class C models is valid for the whole range of laser detunings*. Obviously, this analysis suggests that the value of a used for class A models, should be increased several times to account phenomenologically for the effects of the atom-atom interactions. For class A* models, with $a^*\geqslant 3a$, the theory becomes valid for the whole range of detunings.

(ii) For $T\simeq T_c$ where T_c is the critical temperature for BEC, $N=10^7$, $a=10$ μm one can use class A models with an appropriately scaled size of the Gaussian density profile, $a(\beta_c)$. The critical value of $\beta\omega_t$ for BEC may be estimated to be $(\beta\omega_t)_c\simeq(1.202/N)^{1/3}\simeq 2\times 10^{-2}$ [46,47]. As a result $a(\beta_c)\simeq 100$ μm [from Eq. (38)], and the validity of the theory requires that

$$\max(|\Delta|,\Gamma)>0.02\gamma. \tag{88}$$

The above condition is again fulfilled for all detunings, when $\Gamma\sim\max(\bar{\gamma},\Gamma_d)$. It is interesting to note that even for the idealized model, which neglects completely the spontaneous emission events out of the condensate which disturb the thermal equilibrium, our theory is valid up to detunings of the order of a few hundred $\Gamma\simeq\Gamma_d$.

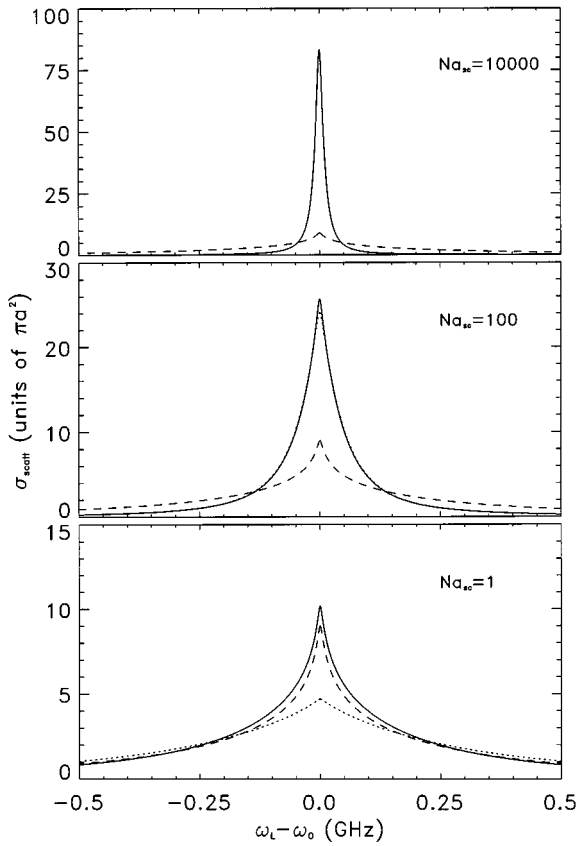

FIG. 6. The same as in Fig. 5(a) but for $\Gamma=\gamma$.

Above the temperature such that $\beta\omega_t \simeq 3\times 10^{-3}$ the theory becomes valid for all detunings for both the idealized, and the more realistic model.

The above estimates are easily translated to another experimentally accessible case, namely microtraps (with $a\simeq 1$ μm) containing $N\simeq 10^4$ atoms.

This discussion shows that generally the results obtained from the GDT are reliable for the whole range of detunings, although at low temperatures one has to use models with realistic density profiles that account for atom-atom interactions and allow for spontaneous emission out of condensate. As we shall see in Sec. VII, the results obtained within the framework of the GDT are numerically very close to those obtained from the on-shell approximation. We thus conjecture that in the regime of parameters of interest both theories give an accurate description of the scattering process. It is worth stressing that our description accounts for nonperturbative multiple scattering effects and provides a complementary approach to the polariton theory of Svistunov and Shlyapnikov [9], and to the single harmonic oscillator approach of Javanainen [11]. More importantly, our approach is valid in the regime of parameters that are expected in many experiments.

Of course, the fact that one considers here the regime in which the effects of the gap in the polariton spectrum are irrelevant does not imply that the present theory does not describe relevant effects due to polariton formation. This is especially true for the idealized model. For such a model in the stationary state there survives some coherent amplitude of the excited-state atoms, which (due to quantum diffusion and drift) is not able to undergo a spontaneous transition to the condensate state. In another words, the incident field produces a coherent combination of the scattered field and excited matter wave – i.e., *polaritons*. The fact that the effective potential in the idealized model is complex, reflects the fact that part of the incident energy is absorbed to excite some atoms and is never returned back to the field. For the model that includes spontaneous emission out of the condensate this energy is returned to field in the form of inelastically scattered photons.

VII. RESULTS AND DISCUSSIONS

In this section we report some of our numerical results. We present cross sections in the parameter range of interest to experiments. We also compare the results obtained from the two approaches discussed in Sec. VI. We discuss also the dependence of the results on the trap size a and on the interaction strength $Na_{\rm sc}/a$.

We start our discussion with the results of the on-shell approximation. In that case the cross sections can be represented as sums of Lorentzian contributions of partial waves [see Eqs. (60) and (62)].

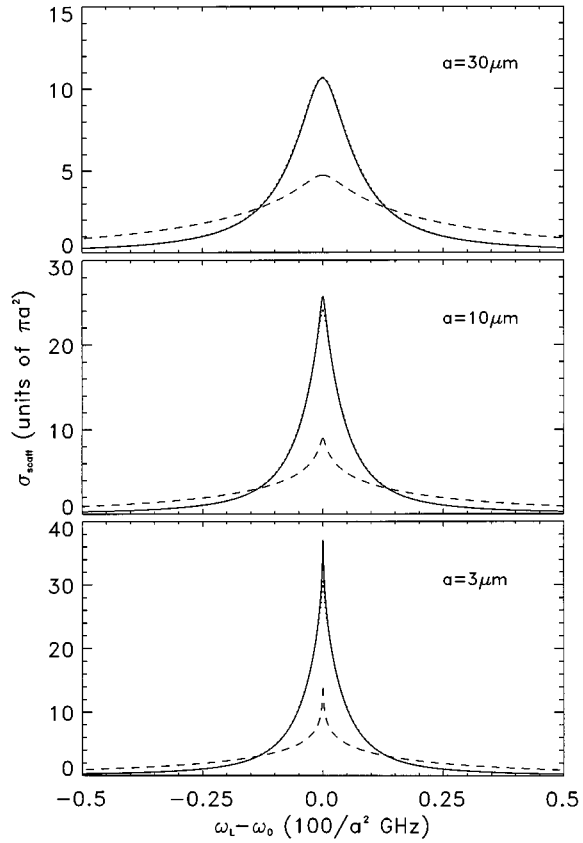

FIG. 7. Comparison of the dependence of the scattering cross section on the trap size for $a=3$, 10, and 30 μm. We have used $Na_{\rm sc}=100$ and $\Gamma=\gamma$. The solid lines represent the results obtained from the density profile of the numerical solutions of the nonlinear Schrödinger equation (42). The dotted lines represent the results obtained for the approximate density profiles given by Eq. (43). The dashed lines serve as a reference and are obtained for noninteracting gases with the Gaussian density profile given by Eq. (36). The dashed lines can also be viewed as representing the high-temperature limit as given by Eq. (37).

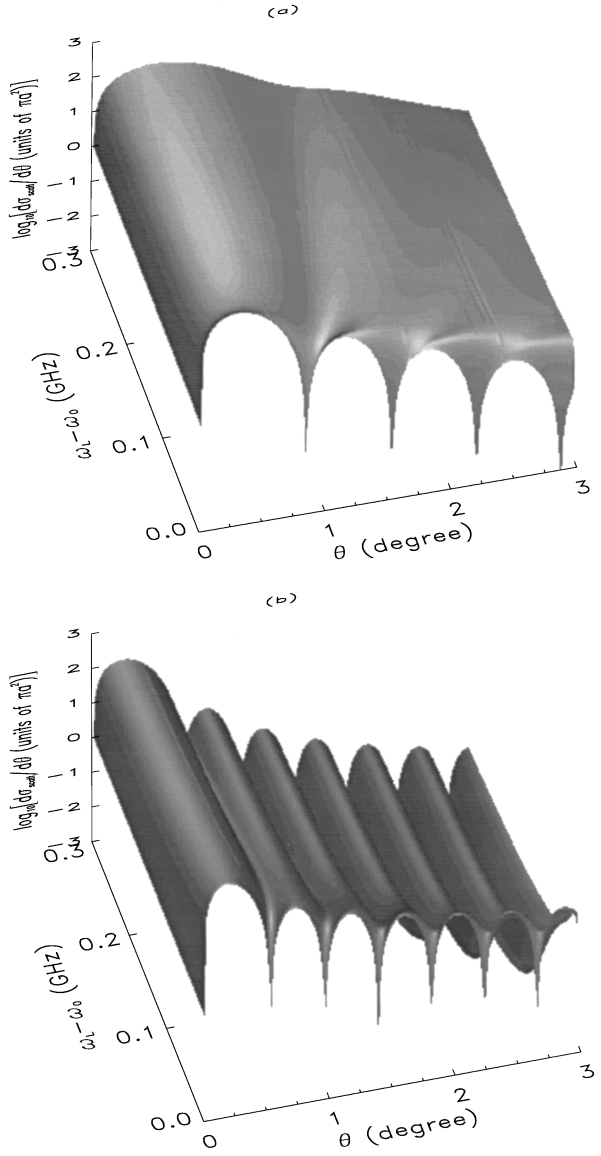

FIG. 8. The spectral-angular distribution of the scattering cross section for $\Gamma=\gamma$ and $a=10\ \mu$m; (a) for a noninteracting gas. (b) Results from the approximate density profile given by Eq. (43) with $Na_{sc}=100$.

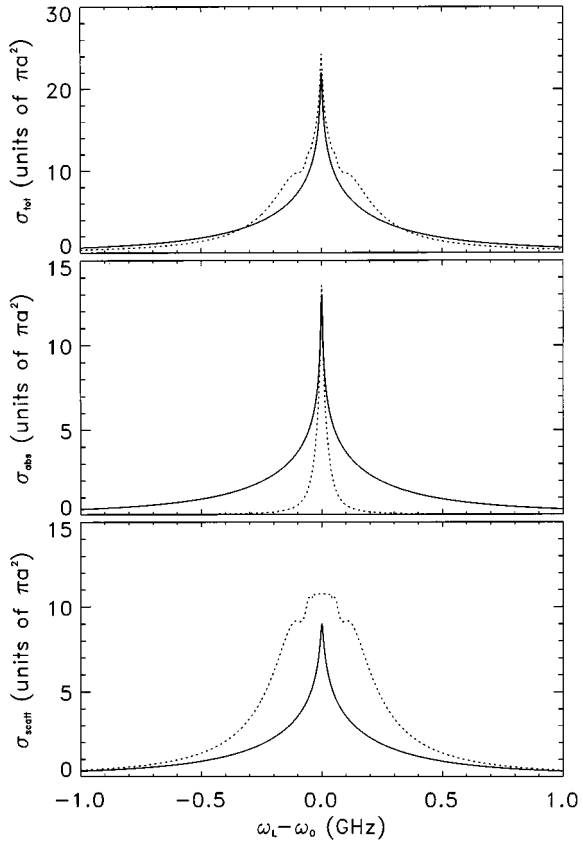

FIG. 9. Comparison between the results of the scattering, absorption, and total cross sections obtained from the on-shell approximation and the GDT for the case of a noninteracting gas with $\Gamma=\gamma$ and $a=10\ \mu$m. The solid lines represents the result obtained from the on-shell approximation, while the dotted line represents the result obtained from GDT.

In Figs. 3 and 4 we have plotted the partial Lorentzian widths γ_L^l[as defined in Eq. (56)] as a function of the order of the spherical harmonics l for three different values of trap sizes (as listed in each figure) and two different interaction strengths. Here, the solid lines represent the results given by Eq. (58) for an ideal noninteracting gas and serve as a reference. The dashed lines represent results for the density profiles obtained from the numerical solutions of the NLSE (42). Finally, the dotted lines represent the results corresponding to the approximate solutions of the NLSE given by Eq. (43).

Note that since the contribution of each Lorentzian to the scattering cross section is proportional to $(\gamma_L^l)^2$, the results in Figs. 3 and 4 can be viewed as a measure of the relative significance of the partial waves.

Figure 3 represents the results of the partial Lorentzian widths for the interaction strength $Na_{sc}/a=1$ when the density profile does not significantly differ from the Gaussian distribution for the noninteracting gas (as given in Fig. 2). In this case the approximate density given by Eq. (43) does not provide a good approximation. In Fig. 4 we present the results for $Na_{sc}/a=10\,000$ when the approximate density of Eq. (43) becomes an excellent approximation.

We notice that generally the number of Legendre polynomials involved (with nonzero partial width) in the scattering increases with the trap size. Comparison of Fig. 3 with Fig. 4 shows that this number increases also with interaction strength [33]. We find that, in general, the exact numerical solution of the NLSE leads to broader partial width distributions than those obtained for noninteracting gases in proportion to the effective size R_0[Eq. (44)]. It is also important to note that the results obtained from the approximate solutions of the NLSE given by Eq. (43) lead to partial width distributions that approximate quite well the results for interacting gases even in the case of moderate coupling strength $Na_{sc}=1$ (Fig. 3). Of course, as the interaction strength increases, it becomes a better and better approximation (see Fig. 2). The results for the cross section can hardly be distinguished then from those obtained from the exact solutions of the NLSE (see Fig. 4).

In Figs. 5–8 we present and discuss parameter dependences of the cross sections obtained from the on-shell ap-

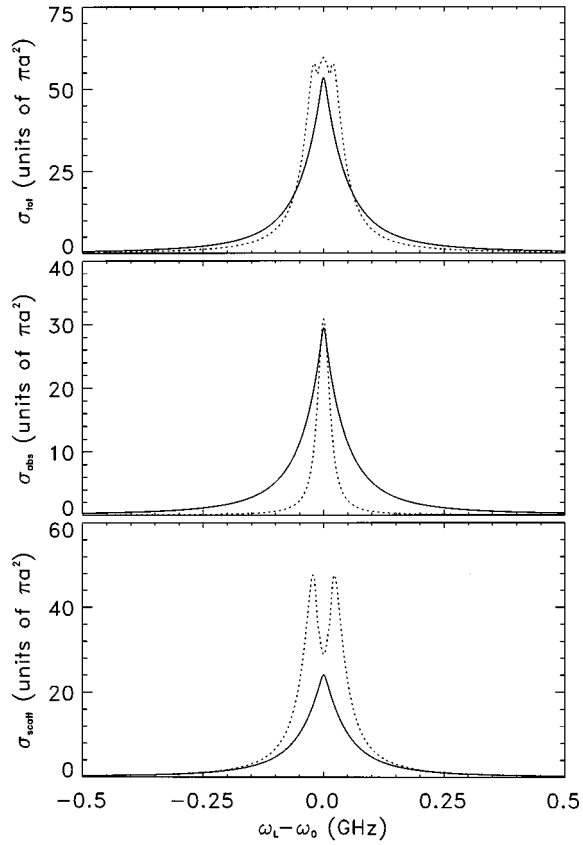

FIG. 10. The same as Fig. 9 but for an interacting condensate with $Na_{sc}=100$. The results obtained with the help of both approaches are calculated with the approximate density profile given by Eq. (43).

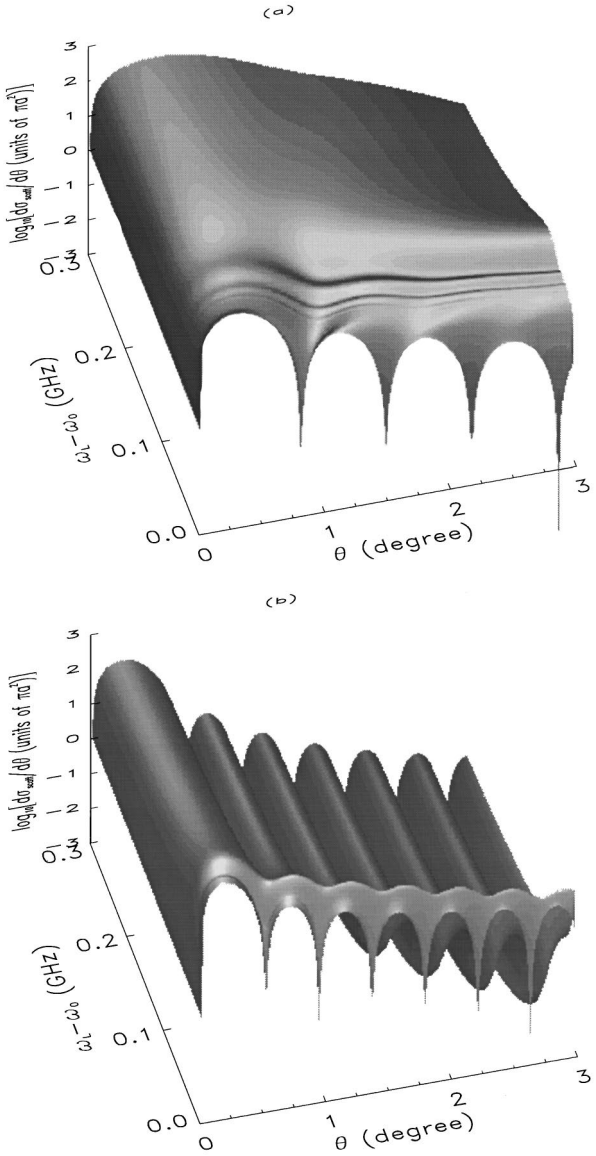

FIG. 11. The same as Fig. 8, but obtained from the GDT approach.

proximation. Unless otherwise stated, from now on we use the convention that the solid lines represent the results obtained from the density profile corresponding to the numerical solutions of the NLSE (42). The dotted lines represent the results obtained from the approximate density profiles given by Eq. (43). Finally, the dashed lines are obtained with the help of the on-shell approximation for noninteracting gases with the Gaussian density profile given by Eq. (36).

Figure 5 represents the scattering cross sections for the three different values of the interaction strength $Na_{sc}/a=10\,000,100$, and 1, respectively. These results were obtained for the idealized model with $\Gamma=ka\omega_t$. For a Cs atom with the mass of about 220 atomic mass units, the trap frequency ω_t is related to the trap size according to $a^2=\hbar/(2M\omega_t)$. For $a=2$ μm, $\omega_t=10$ Hz. Therefore for the three different sizes used the corresponding values for $\Gamma=ka\omega_t$ are 105, 31.4, and 10.5 Hz. We remind the reader that these results may be alternatively viewed as corresponding to scattering of light at a very narrow resonance (for instance, a forbidden transition for which γ is very small).

From Fig. 5 we see clearly that the line shapes have two basic features: an overall broad spectrum of the effective collective width $\propto N\gamma/(k_L a)^2$, and a narrow feature close to the resonance of width comparable to Γ. We notice also that with the increase of the interaction strength Na_{sc}/a, the overall cross sections calculated from the approximate density profiles become indistinguishable from those obtained with the exact density distribution [Fig. 5(a)]. However, very close to resonance [Fig. 5(b)], the abrupt edge in the approximate density profile solutions affects the contribution of the higher partial waves (compare Fig. 3). As a result the central feature is much less pronounced for the approximate solutions. As we see in Fig. 6, these artificial differences between the solid and dotted curves vanish for larger values of $\Gamma\simeq\gamma$.

The overall shape and the magnitude of the cross sections also change with the interaction strength, as shown in Fig. 5. Larger values of interaction strength lead to larger R_0, and consequently to broader spatial distributions with a smaller density in the trap center. The collective width therefore becomes smaller as represented in Figs. 5(a) and 6. For the same reason the magnitudes of various cross sections increase with the interaction strength. However, we find that the increase does not scale as πR_0^2 (as a simple geometrical argument would suggest). Instead, the cross section is a rather complex function of the parameter Na_{sc}. Similar results as in Fig. 5(a) are displayed in Fig. 6 for $\Gamma=\gamma$. As we

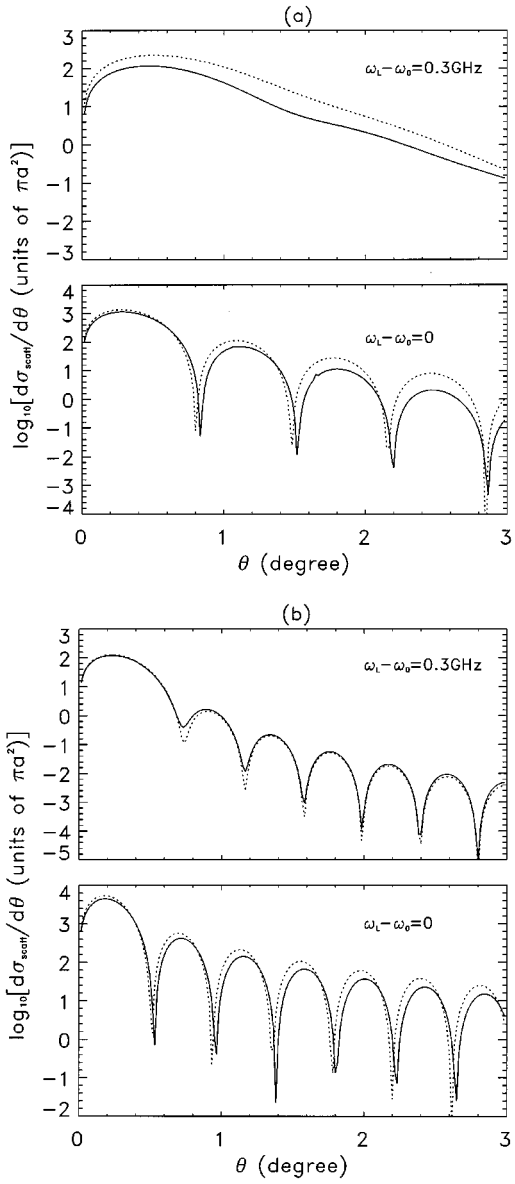

FIG. 12. Comparison of the angular scattering cross sections at two fixed laser detunings for results obtained from the GDT and on-shell approximations. The solid lines represent the results from the on-shell approximation, while the dotted lines represent the results from the GDT; (a) line sections of Fig. 8(a) and Fig. 11(a) for the noninteracting density profile; (b) line sections of Fig. 8(b) and Fig. 11(b) for the approximate density profile for $Na_{sc}=100$.

already mentioned, in this case the agreement between the results corresponding to the exact and approximate solutions of the NLSE is much better. We stress that the dependence of the cross sections on the interaction strength has an analogous form for other trap sizes ($a=3,30$ μm [33]).

In Fig. 7 we compare the dependence of the scattering cross sections on the trap size for an interaction strength $Na_{sc}/a=100$ and $\Gamma=\gamma$. For a better comparison, we have scaled the frequency coordinate by $[10(\mu\text{m})/a]^2$ to eliminate the asymptotic density dependence of the cross sections. We observe again that the results obtained from the approximate density profile agree with those from the exact density profile very well. Similar conclusions hold for other values of the interaction strength [33]. As discussed in Sec. V, within the on-shell approximation, the absorption cross section is roughly the same as the scattering cross section for most of the parameter regions of practical interest. For this reason we do not display comparative results for the absorption cross sections here.

In Fig. 8 we have plotted the spectral-angular distribution, i.e., differential scattering cross sections for $\Gamma=\gamma$ and $a=10$ μm. As we see, the scattering is basically restricted in the forward direction to a solid angle determined by the size of the condensate. In Fig. 8(a) we have plotted the results for the case of an ideal noninteracting gas. Close to resonance the angular distribution displays patterns of oscillations due to the interference of all the harmonics involved in the scattering. The period of those oscillations is proportional to $1/(k_L a)$. Off resonance these oscillations decay very rapidly as higher order harmonics contribute less and less. Note that the plot is on a logarithmic scale. In Fig. 8(b) the same result is presented for the case of an interacting gas with $Na_{sc}/a=100$. The repulsive interaction increases the size of condensate, and consequently the oscillation period becomes smaller, in proportion to $\propto 1/(k_L R_0)$. Interestingly, the oscillations in the angular dependence can now be seen even far off-resonance. Analogous results hold for different trap sizes and different interaction strengths [33].

In Figs. 9 and 10 we present a comparison between the results obtained from the on-shell approximation and those obtained from the generalized diffraction theory for the scattering, absorption, and total cross sections. As we can see in Fig. 9 for the noninteracting case, the overall agreement between the two approaches is reasonably good. This is especially true for the total cross section. Note that on resonance the total cross sections obtained from both approaches have roughly the same magnitude, and the respective spectral wings merge together.

We should stress, however, that the agreement between the scattering cross section and absorption cross sections is not very good. In particular the GDT predicts that the scattering cross section is broader than the absorption cross section. In the on-shell approximation, on the other hand, the scattering and absorption cross sections have the same width. Moreover, the scattering cross section obtained from the GDT exhibits interesting (although relatively broad) structures close to resonance. Note, however, that the narrow peak at the exact resonance is still present in the absorption cross section.

Figure 10 presents similar results as Fig. 9, but now for an interacting condensate with $Na_{sc}/a=100$. Both results were obtained from the approximate density profile given by Eq. (43). We note that now there exists an additional structure ''line splitting'' in the scattering cross section obtained from the GDT close to the line center. This is in fact a general feature of the results obtained from the GDT. It is not yet fully understood, and will be discussed elsewhere [33]. At this point it is worthwhile to point out that in contrast to the on-shell approximation, the GDT includes contributions that are not fully coherent in a similar manner to the way Mollow spectrum has both coherent and incoherent component at the laser frequency [34]. We stress also that the shape of the absorption cross section is governed by the relevant dissipative processes, and for both approaches exhibit a narrow

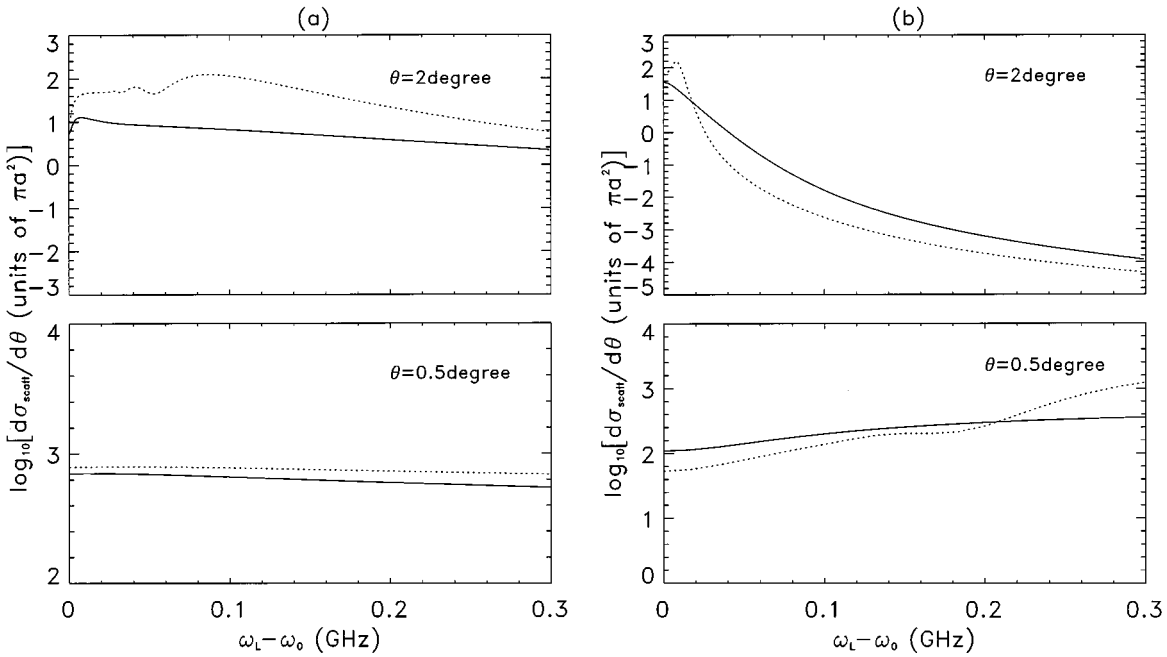

FIG. 13. Comparison of the frequency dependence of the scattering cross sections at two fixed polar angles for results obtained from the GDT and on-shell approximations. The solid lines represent the results from the on-shell approximation, while the dotted lines represent the results from the GDT; (a) line sections of Fig. 8(a) and Fig. 11(a) for the noninteracting density profile; (b) line sections of Fig. 8(b) and Fig. 11(b) for the approximate density profile given by Eq. (43) for $Na_{sc}=100$.

peak at the resonance of width Γ.

In Fig. 11 we present the spectral-angular distributions (i.e., differential cross sections) obtained from GDT. Here the same parameters have been used as in Fig. 8. As we see the agreement between the two approaches is qualitatively very good. For a clear comparison, we also display in Figs. 12 and 13 a few line sections from the surface plots of Figs. 8 and 11. In Fig. 12, we present the angular distributions at two fixed detunings. In Fig. 13 the comparison of the scattering cross sections is made for two fixed polar angles.

Even though the differences between the two approaches are sometimes clearly visible, we conclude that in general the two approximate theories agree reasonably well in terms of magnitudes of the cross sections close to resonance, overall shape of the spectra (narrow feature in the center with a broad background), widths of the spectra, etc. This conclusion holds for other trap sizes and interaction strengths as well. This suggests that the parameter ranges of applicability of the two methods are similar.

VIII. CONCLUSIONS

In summary we have calculated the line shapes for coherent scattering from a BEC. This line shape has three interesting properties. First, it exhibits a very broad resonance of width of order $\gamma_{\text{eff}}=3N\gamma/2(k_La)^2$. To detect this resonance it will be sufficient to shine strongly detuned light on the system of cooled atoms, with a detuning of the order of γ_{eff}. Those atoms that are not in the condensate phase will Rayleigh scatter with a cross section with effective linewidth $\gamma(\ll\gamma_{\text{eff}})$ and will not significantly contribute, while the condensed atoms will scatter collectively. Second, the very narrow feature ($\sim\Gamma$) in the spectrum at $\omega_L\simeq\omega_0$ suggests obvious applications of this system for precision spectroscopy. This is one of the comparatively rare examples of a situation in which such a narrow resonance is present. (The Dicke narrowed spectrum [43] is also similar in shape to this sharp spectral feature.) Yet the response of the system at this resonance is strong. This is in contrast to normal narrow resonances associated with weak transitions. From the experimental point of view, the spike at $\omega_L\simeq\omega_0$ is especially interesting, since it will not be smeared out due to fluctuations in the number of condensed atoms. Third, the line shape is non-Lorentzian, and in some circumstances may exhibit additional interesting features. In particular the GDT predicts line splitting and similar structures in the scattering cross section close to resonance. Although at present those features are not fully understood, we point out that they arise in the GDT from the contributions that are not fully coherent.

We emphasize again that coherent scattering probes in the first place the density profile of the trapped atoms, and does not reflect quantum statistical effects directly. It does reflect these effects indirectly, however, through the density profiles that are different for bosons or fermions at low temperatures. It also reflects the very fact of condensation, since the density profile changes in the condensation process. As we pointed out earlier, our results for broad Gaussian density profiles may be in principle regarded as corresponding to high-temperature cases. According to our theory, in both cases of a low-temperature BEC and a high-temperature gas the scattering will occur mainly in the forward direction. *Thus, forward scattering is not a signature of BEC.* In the high-temperature case, however, the divergence of the scattered beam will be determined by the thermal size $a_{\text{th}}\sim a(\beta)$ [Eq. (38)] of the sample, i.e., it will be proportional to $1/[k_La(\beta)]$, and thus much smaller than the angle in the presence of the condensate [since $a(\beta)\gg\lambda$].

The quantum statistical effects are clearly visible in the spectrum of scattered light, since they cause an enhancement of the spontaneous emission rate into the condensate. These effects again will cease to exist for a gas at temperatures above the Bose-Einstein transition; the spectrum of coherent scattering will be then much narrower, and in the extreme limit $\beta\to 0$ it will tend to be Lorentzian with a width $\sim\Gamma$, bounded from below by the single atom spontaneous emission rate γ or by the rate Γ_d due to single atom quantum diffusion processes. The spectrum in the presence of the condensate at low temperatures will display a broad *non-Lorentzian* shape gradually narrowing toward the resonance, and transforming into a narrow feature of the characteristic width Γ in close vicinity to the resonance. Physically, the narrowing of the spectrum close to resonance comes from the fact that the quantum statistical enhancement of the spontaneous emission rate to the condensate decreases with successive multiple scattering events due to the broadening of excited atomic wave packet in momentum space (or alternatively, due to the excitation of higher and higher partial wave components). Even though the narrow feature in the spectrum at low temperatures reminds one somewhat of the Lorentzian spectrum at high temperatures, it is worth stressing that both its magnitude and shape strongly depend on the sample size a, and therefore on temperature (compare Fig. 7) [44].

According to the present study the clear signatures of condensation from coherent light scattering are thus: (a) forward scattering with a divergence angle proportional to $1/(k_L a)$ determined by the size of the condensate a; (b) a broad non-Lorentzian spectrum with an overall width of $\sim N\gamma/(k_L a)^2$ in the spectral wings, a gradually narrowing width closer to the resonance, and a characteristic width $\sim\Gamma$ at the resonance.

ACKNOWLEDGMENTS

We acknowledge very fruitful discussions with K. Burnett, Y. Castin, I. Cirac, E. Cornell, A. Dalgarno, J. Dalibard, E. Heller, M. Jamieson, J. Javanainen, V. Kharchenko, G. Shlyapnikov, and P. Zoller. The idea of this work was born at the BEC Seminar at JILA, and we thank all members of that seminar for enlightening discussions and comments. The work of L.Y. and M.L. was supported by the NSF through a grant to the Institute for Theoretical Atomic and Molecular Physics at Harvard University and the Smithsonian Astrophysical Observatory. M.L. was also supported by the NSF and Polish Academy of Sciences Grant No. INT-9023548. J.C. was supported by NSF Grant No. PHY90-12244 through the University of Colorado.

APPENDIX A: DEFINITION OF THE SCATTERING CROSS SECTION

Within the on-shell approximation, the solution of the scattering equation (8) has the form

$$a_{\vec{k}\mu}(t\to\infty)\sim\alpha\delta(\vec{k}-\vec{k}_L)\,\delta_{\mu\mu_L}e^{-i\omega_L t}+\alpha B(\vec{k},\mu)\,\delta(ck-\omega_L)e^{-i\omega_L t},\qquad\text{(A1)}$$

from which we can define the scattering cross section according to the following scheme. The number of scattered photons $dn_{\rm scatt}$ and the number of incident photons are given, respectively, by

$$dn_{\rm scatt}\propto d\Omega_{\vec{k}}\sum_\mu\int_0^\infty|\alpha B(\vec{k},\mu)|^2\delta^2(ck-\omega_L)k^2\rho(k)dk,\qquad\text{(A2)}$$

$$n_{\rm in}\propto\int|\alpha|^2\delta^2(\vec{k}-\vec{k}_L)\rho(k)d\vec{k}.\qquad\text{(A3)}$$

Therefore the differential scattering cross section can be defined as

$$\frac{d\sigma_{\rm scatt}}{d\Omega_{\vec{k}}}=\frac{dn_{\rm scatt}}{n_{\rm in}}=(\pi a^2)\frac{4\pi}{(k_L a)^2}\left(\frac{k_L^2}{c}\right)^2\sum_\mu|B(\vec{k},\mu)|^2_{k=k_L},\qquad\text{(A4)}$$

where we have used the standard normalization,

$$\delta^2(\vec{k}-\vec{k}_L)=\frac{1}{(2\pi)^3}(c\tau_d)\mathscr{A}\delta(\vec{k}-\vec{k}_L),\qquad\text{(A5)}$$

$$\delta^2(ck-\omega_L)=\frac{1}{c^2}\frac{1}{2\pi}(c\tau_d)\,\delta(k-k_L).\qquad\text{(A6)}$$

Here $\mathscr{A}$ is the unit cross-sectional area corresponding to the incident flux, and τ_d is the duration of the incident weak field pulse. The differential cross section in units of πa^2 is, therefore,

$$\frac{d\sigma_{\rm scatt}}{d\Omega_{\vec{k}}}=\frac{4\pi}{(k_L a)^2}\left(\frac{k_L^2}{c}\right)^2\sum_\mu|B(\vec{k},\mu)|^2_{k=k_L}.\qquad\text{(A7)}$$

Note that according to this normalization, the cross section is 4π times bigger than what we have used in Ref. [12].

An optical theorem can be derived by squaring Eq. (A1), and calculating the total number of photons $n_{\rm ph}$ in the scattered field. In the remote past when $t\to-\infty$, the number of photons in the field is $n_{\rm in}$. Conservation of energy then gives

$$n_{\rm in}=n_{\rm ph}+n_{\rm abs}.\qquad\text{(A8)}$$

We have denoted the number of photons absorbed by $n_{\rm abs}$, and $n_{\rm ph}$ is the number of photons remaining in the field in the long time limit. A corresponding absorption cross section can be defined in a form similar to Eq. (A4) for the scattering cross section. In the long time limit when $t\to\infty$,

$$n_{\rm ph} \propto \sum_{\mu} \int |\alpha \delta(\vec{k}-\vec{k}_L)\delta_{\mu\mu_L} e^{-i\omega_L t} + \alpha B(\vec{k},\mu)\delta(ck-\omega_L)e^{-i\omega_L t}|^2 \rho(k) d\vec{k}$$

$$= n_{\rm in} + \int dn_{\rm scatt} + 2\ {\rm Re}[|\alpha|^2 B(\vec{k}_L,\mu_L)\delta(ck-\omega_L)\rho(k_L)]. \quad \text{(A9)}$$

Substituting Eq. (A9) into Eq. (A8), and using again the normalization relation (A6), we obtain the total cross section (for cross sections in units of πa^2)

$$\sigma_{\rm tot} = \sigma_{\rm scatt} + \sigma_{\rm abs} = -\frac{8\pi}{(k_L a)^2}\frac{k_L^2}{c}\,{\rm Re}[B(\vec{k}_L,\mu_L)]. \quad \text{(A10)}$$

Comparing the above expression with Eq. (72), we see that $-iB(\vec{k},\mu_L)$ can be associated with a scattering amplitude, and in particular

$$-\frac{8\pi^2}{c}\,{\rm Re}[B(\vec{k}_L,\mu_L)] \to \frac{4\pi}{k_L}\,{\rm Im}[f(\vec{k}_L,\vec{k}_L)]. \quad \text{(A11)}$$

APPENDIX B: SPONTANEOUS EMISSION OUT OF THE CONDENSATE

In this Appendix we show that the spontaneous emission out of the condensate can be included in the theory by replacing ω_0 by $\omega_0 - i\bar{\gamma}$, with $\bar{\gamma}$ being typically of the order of the natural linewidth γ. As a result, the effective decay constant of the self-energy kernel becomes of the order of $\bar{\gamma}+\Gamma_d$. Thus, in the regime when $\Gamma_d \ll \gamma$, Γ becomes comparable to γ.

We consider here only the class A model with a Gaussian density profile at $T=0$, and zero potential in the excited state. We employ the Schrödinger equation approach to describe single photon scattering events in the spirit of the one-photon approximation [48]. The wave function contains in this case three components

$$|\Psi(t)\rangle = \sum_{\mu}\int d\vec{k}\,\alpha(t;\vec{k},\mu)|N,0,\ldots;\vec{0};\vec{k}\mu\rangle + \sum_{\vec{m}}\vec{\beta}_{\vec{m}}(t)\cdot\vec{e}^{\dagger}_{\vec{m}}|N-1,\ldots;\vec{0};0\rangle + \sum_{\vec{n}\neq 0}\sum_{\mu}\int d\vec{k}\,\gamma_{\vec{n}}(t;\vec{k},\mu)|N-1,\ldots,1,\ldots;\vec{0};\vec{k}\mu\rangle, \quad \text{(B1)}$$

where the indices for the Fock representation of the wave function are arranged in the following order $|{\rm ground;excited;photon}\rangle$, and $|N,0,\ldots;\vec{0};\vec{k}\mu\rangle$ denotes the state for which all N atoms are in the condensate (i.e., in the ground electronic state and in the ground state of the trap), and a photon of momentum $\vec{k}$ and polarization $\vec{\epsilon}_{\vec{k}\mu}$ is present; $\vec{e}^{\dagger}_{\vec{m}}|N-1,\ldots;\vec{0};0\rangle$ is a state for which $N-1$ atoms are in the condensate, one atom is excited to the state $\vec{m}$, and there are no photons; and, finally, $|N-1,\ldots,1,\ldots;\vec{0};\vec{k}\mu\rangle$ is a state for which $N-1$ atoms are in the condensate, one atom is in the ground electronic state, but in the $\vec{n}$th excited state of the trap, and a photon of momentum $\vec{k}$ and polarization $\vec{\epsilon}_{\vec{k}\mu}$ is present.

The Schrödinger equations for the amplitudes can be easily derived from the Hamiltonian (1), and they are

$$\dot{\alpha}(t;\vec{k},\mu) = -ick\alpha(t;\vec{k},\mu) - i\sqrt{N}\sum_{\vec{m}}\rho(k)\,\eta_{0\vec{m}}(\vec{k})[\vec{\epsilon}_{\vec{k}\mu}\cdot\vec{\beta}_{\vec{m}}(t)], \quad \text{(B2)}$$

$$[\vec{\epsilon}_{\vec{k}\mu}\cdot\dot{\vec{\beta}}_{\vec{m}}(t)] = -i(\omega_0 + E^e_{\vec{m}})[\vec{\epsilon}_{\vec{k}\mu}\cdot\vec{\beta}_{\vec{m}}(t)] - i\sqrt{N}\sum_{\mu'}\int d\vec{k}'\rho(k')[\eta_{0\vec{m}}(\vec{k}')]^*(\vec{\epsilon}_{\vec{k}\mu}\cdot\vec{\epsilon}_{\vec{k}'\mu'})\alpha(t;\vec{k}',\mu') - i\sum_{\vec{n}\neq 0}\sum_{\mu'}\int d\vec{k}'\rho(k')[\eta_{\vec{n}\vec{m}}(\hat{k}')]^*(\hat{\epsilon}_{\vec{k}\mu}\cdot\hat{\epsilon}_{\vec{k}'\mu'})\gamma_{\vec{n}}(t;\hat{k}',\mu'), \quad \text{(B3)}$$

$$\dot{\gamma}_{\vec{n}}(t;\vec{k},\mu) = -i(ck + E^g_{\vec{n}})\gamma_{\vec{n}}(t;\vec{k},\mu) - i\sum_{\vec{m}}\rho(k)\,\eta_{\vec{n}\vec{m}}(\vec{k})[\vec{\epsilon}_{\vec{k}\mu}\cdot\vec{\beta}_{\vec{m}}(t)], \quad \text{(B4)}$$

with $\alpha(0;\vec{k},\mu) = \delta(\vec{k}-\vec{k}_L)\delta_{\mu\mu_L}$, $\vec{\beta}_{\vec{m}}(0)=0$, and $\gamma_{\vec{n}}(0;\vec{k},\mu)=0$. If we had ignored $\gamma_{\vec{n}}(t,\vec{k},\mu)$ in the above equations, the Eqs. (B2) and (B3) would be equivalent to the linearized Heisenberg equations discussed in Sec. II. In particular, $\alpha(t;\vec{k},\mu)$ would

have fulfilled the scattering equation (8). In general, we use the Laplace-transform technique to solve Eq. (B4) for $\gamma_{\vec{n}}(s;\vec{k},\mu)$, and then insert it into the solution for the Laplace-transformed Eq. (B3). The result is

$$[s+i(\omega_0+E^e_{\vec{m}})][\vec{\epsilon}_{\vec{k}\mu}\cdot\vec{\beta}_{\vec{m}}(s)]=-i\sqrt{N}\sum_{\mu'}\int d\vec{k}'\rho(k')[\eta_{0\vec{m}}(\vec{k}')]^*(\vec{\epsilon}_{\vec{k}\mu}\cdot\vec{\epsilon}_{\vec{k}'\mu'})\alpha(s;\vec{k}',\mu')$$
$$-\sum_{\vec{m}'}\sum_{\mu'}\int d\vec{k}'|\rho(k')|^2\sum_{\vec{n}\neq 0}\frac{[\eta_{\vec{n}\vec{m}}(\vec{k}')]^*\eta_{\vec{n}\vec{m}'}(\vec{k}')}{s+i(E^g_{\vec{n}}+ck')}(\vec{\epsilon}_{\vec{k}\mu}\cdot\vec{\epsilon}_{\vec{k}'\mu'})[\vec{\epsilon}_{\vec{k}'\mu'}\cdot\vec{\beta}_{\vec{m}'}(s)]. \quad \text{(B5)}$$

To get an estimate of the role of the last term in Eq. (B5) we use the Wigner-Weisskopf pole approximation [49] and replace $s+iE^g_{\vec{n}}+ick'$ with $i(ck'-\omega_0+E^g_{\vec{n}}-E^e_{\vec{m}})+\varepsilon$, with an infinitesimally small $\varepsilon>0$ in the denominator. We also substitute $E^e_{\vec{m}}-E^g_{\vec{n}}=k_L^2/2M$, since the numerator does not vary much with the change of $E^e_{\vec{m}}$ or $E^g_{\vec{n}}$. Then we employ the sum rule

$$\sum_{\vec{n}\neq 0}[\eta_{\vec{n}\vec{m}}(\vec{k})]^*\eta_{\vec{n}\vec{m}'}(\vec{k}')=\delta_{\vec{m}\vec{m}'}-[\eta_{0\vec{m}}(\vec{k}')]^*\eta_{0\vec{m}'}(\vec{k}). \quad \text{(B6)}$$

Since both $[\eta_{0\vec{m}}(\vec{k}')]^*$ and $\eta_{0\vec{m}'}(\vec{k}')$ are sharply peaked at $\vec{m}\simeq\vec{m}'\simeq\vec{k}'$, and (at least for not too small traps, $a\geqslant\lambda$), the approximate momentum conservation allows us to limit our attention to $\vec{m}\simeq\vec{k}_L$. We can thus approximate

$$[\eta_{0\vec{m}}(\vec{k}')]^*\eta_{0\vec{m}'}(\vec{k}')\vec{\beta}_{\vec{m}'}(s)\simeq[\eta_{0\vec{k}_L}(\vec{k}')]^*\eta_{0\vec{m}'}(\vec{k}')\vec{\beta}_{\vec{m}}(s). \quad \text{(B7)}$$

Neglecting the polarization dependence as discussed in the on-shell approximation in Sec. V, we obtain the equation

$$[s+i(\omega_0+E^e_{\vec{m}})+\bar{\gamma}]\vec{\beta}_{\vec{m}}(s)$$
$$=-i\sqrt{N}\sum_{\mu}\int d\vec{k}\rho(k)[\eta_{0\vec{m}}(\vec{k})]^*\vec{\epsilon}_{\vec{k}\mu}\alpha(s;\vec{k},\mu), \quad \text{(B8)}$$

which is valid for $\vec{m}\simeq\vec{k}_L$, where

$$\bar{\gamma}\simeq\gamma\left[1-\frac{3}{2\sqrt{2}(k_La)^2}\right]. \quad \text{(B9)}$$

Physically, the above formula means that the rate of spontaneous emission out of the condensate is smaller than the natural linewidth by an amount that is of the order of the rate of emission back to the ground state containing a single atom. The latter quantity is smaller than γ, since due to approximate momentum conservation, such emission is limited to the solid angle determined by the size of the ground-state wave function. Equation (B8) proves our conjecture that the processes of spontaneous emission out of the condensate can be accounted for by the simple substitution $\omega_0\rightarrow\omega_0-i\bar{\gamma}$, as is normally used for the one-photon approximation [48].

APPENDIX C: SELF-ENERGY KERNEL AT FINITE TEMPERATURE

In this appendix we demonstrate that the reduced self-energy kernel can be approximated by Eq. (14) at finite T $(\neq 0)$. For simplicity, we first consider class A models with the same trapping potential for the ground and excited atoms, but the results are expected to be valid generally. Using the series expansion for expression (7)

$$N_{\vec{n}}=\sum_{l=1}^{\infty}\mathcal{Z}^l\exp(-l\beta E^g_{\vec{n}}), \quad \text{(C1)}$$

we can represent the reduced kernel (12) in the form

$$\tilde{\mathscr{L}}(s;\vec{k},\vec{k}')=\sum_{l=1}^{\infty}\mathcal{Z}^l\tilde{\mathscr{L}}_l(s;\vec{k},\vec{k}'), \quad \text{(C2)}$$

where

$$\tilde{\mathscr{L}}_l(s;\vec{k},\vec{k}')=\sum_{\vec{n},\vec{m}}\int_0^{\infty}dt e^{-[s+i(E^e_{\vec{m}}+\omega_0-E^g_{\vec{n}})]t}e^{-l\beta E^g_{\vec{n}}}\eta_{\vec{n}\vec{m}}(\vec{k})$$
$$\times[\eta_{\vec{n}\vec{m}}(\vec{k}')]^*. \quad \text{(C3)}$$

Denoting by $\vec{b}=(b_x,b_y,b_z)$ $(\vec{b}^\dagger)$ the annihilation (creation) operators for a single harmonic oscillator describing motion in the trap potential, we introduce

$$\mathscr{H}_h=\omega_t\vec{b}^\dagger\cdot\vec{b}, \quad \text{(C4)}$$

$$\vec{R}=a(\vec{b}+\vec{b}^\dagger), \quad \text{(C5)}$$

$$\vec{R}(t)=e^{-i\mathscr{H}_ht}\vec{R}e^{i\mathscr{H}_ht}=a(\vec{b}e^{i\omega_t t}+\vec{b}^\dagger e^{-i\omega_t t}). \quad \text{(C6)}$$

Using the above notation and the definition of the Franck-Condon factors we can rewrite the expression (C3) in a more compact form

$$\tilde{\mathscr{L}}_l(s;\vec{k},\vec{k}')=\int_0^{\infty}dt e^{-(s+i\omega_0)t}\,\mathrm{Tr}(e^{-l\beta\mathscr{H}_h}e^{-i\vec{k}\cdot\vec{R}}e^{i\vec{k}'\cdot\vec{R}(t)}), \quad \text{(C7)}$$

where Tr() denotes the trace of an operator.

The trace can be easily evaluated using the same methods as described in Appendixes B, C, and D of paper II. The exponents of position operators can be ordered normally with the help of the Baker-Hausdorf formula, while the trace is performed using coherent states. The result is

$$\mathrm{Tr}[e^{-l\beta\mathscr{H}_h}e^{-i\vec{k}\cdot\vec{R}}e^{i\vec{k}'\cdot\vec{R}(t)}]=\frac{1}{(1-e^{-l\beta\omega_t})^3}\exp\left(-\frac{[k^2+(k')^2]a^2(e^{-l\beta\omega_t}+1)-2\vec{k}\cdot\vec{k}'a^2(e^{-i\omega_t t}+e^{-l\beta\omega_t+i\omega_t t})}{2(1-e^{-l\beta\omega_t})}\right). \quad \text{(C8)}$$

We now proceed as in Sec. III, i.e., we expand the above expression up to the second-order terms in t in the exponent. We obtain

$$\tilde{\mathscr{G}}_l(s;\vec{k},\vec{k}')=\frac{1}{(1-e^{-l\beta\omega_t})^3}\exp\left[-\frac{(\vec{k}-\vec{k}')^2a^2(1+e^{-l\beta\omega_t})}{2(1-e^{-l\beta\omega_t})}\right]\int_0^\infty dt e^{-\mathscr{P}_2(l)t^2-\mathscr{P}_1 t}, \quad \text{(C9)}$$

with

$$\mathscr{P}_2(l)=\vec{k}\cdot\vec{k}'a^2\omega_t^2\frac{1+e^{-l\beta\omega_t}}{2(1-e^{-l\beta\omega_t})}$$

$$\simeq k_L^2a^2\omega_t^2\frac{1+e^{-l\beta\omega_t}}{2(1-e^{-l\beta\omega_t})}, \quad \text{(C10)}$$

$$\mathscr{P}_1=s+i\omega_0+i\omega_t\vec{k}\cdot\vec{k}'a^2$$

$$\simeq s+i\omega_0+ik_L^2/2M. \quad \text{(C11)}$$

In principle $\mathscr{P}_2(l)$ is l dependent. For very low temperatures, however, this dependence is negligible. For high temperatures only the term $l=1$ contributes to the kernel. In both these cases we recover the form of Eq. (14) for the kernel using the asymptotic expansion of the error function as in Sec. III. We also use the identity

$$\bar{\rho}(\vec{k}-\vec{k}')=\sum_{l=1}^\infty\frac{z^l}{(1-e^{-l\beta\omega_t})^3}\times\exp\left[-\frac{(\vec{k}-\vec{k}')^2a^2(1+e^{-l\beta\omega_t})}{2(1-e^{-l\beta\omega_t})}\right]. \quad \text{(C12)}$$

For intermediate temperatures, when the resonance line at ω_0 is broadened by $\bar{\gamma}$ (see Appendix B) we can still neglect the l dependence of $\mathscr{P}_2(l)$ (by considering only the $l=1$ term) since typically $\sqrt{\mathscr{P}_2(l)}\ll\bar{\gamma}$. If the natural linewidth γ is small, we replace $\mathscr{P}_2(l)$ by $\pi\Gamma^2/4$ defined according to

$$\frac{2}{\sqrt{\pi}\Gamma}=(1-z)\sum_{l=1}^\infty z^l\frac{1}{\sqrt{\mathscr{P}_2(l)}}. \quad \text{(C13)}$$

The above definition for Γ assures that at exact resonance $(\omega_L-\omega_0-\omega_t k_L^2a^2=0)$ the expression (14) is exact for $\vec{k}=\vec{k}'$.

The above results can be generalized to the case of zero potential in the excited state. Under such an assumption we first note that

$$\eta_{\vec{n}\vec{m}}(\vec{k})=\Psi_{\vec{n}}(\vec{k}-\vec{m}), \quad \text{(C14)}$$

where $\Psi_{\vec{n}}(\vec{k})$ are the normalized harmonic oscillator wave functions in the momentum representation (and once again we use $\vec{m}$ to index the momentum of the center-of-mass motion in the excited state). The reduced kernel can be written again in the form Eq. (C2) with

$$\tilde{\mathscr{G}}_l(s;\vec{k},\vec{k}')=\sum_{\vec{n}}\int d\vec{m}\int_0^\infty dt e^{-[s+i(\omega_t\vec{m}^2a^2+\omega_0)]t}e^{-(l\beta-it)E_{\vec{n}}^g}\Psi_{\vec{n}}(\vec{k}-\vec{m})\Psi_{\vec{n}}^*(\vec{k}'-\vec{m}). \quad \text{(C15)}$$

Introducing $\tilde{\beta}_l(t)=l\beta-it$, we can express the sum over $\vec{n}$ in the above equation as

$$\sum_{\vec{n}}e^{-\tilde{\beta}_l(t)\mathscr{H}_h}\Psi_{\vec{n}}(\vec{k}-\vec{m})\Psi_{\vec{n}}^*(\vec{k}'-\vec{m})=G[\tilde{\beta}_l(t);\vec{k}-\vec{m},\vec{k}'-\vec{m}], \quad \text{(C16)}$$

where $G(.;.,.)$ is the harmonic oscillator temperature Green function in the momentum representation, calculated at complex $\tilde{\beta}_l(t)$. It is given by [50]

$$G[\tilde{\beta}_l(t);\vec{k}-\vec{m},\vec{k}'-\vec{m}]=\left(\frac{a^2}{\pi\sinh[\tilde{\beta}_l(t)\omega_t]}\right)^{3/2}\exp[3\omega_t\tilde{\beta}_l(t)/2]$$

$$\times\exp\left\{-\frac{a^2}{\sinh[\omega_t\tilde{\beta}_l(t)]}\{[(\vec{k}-\vec{m})^2+(\vec{k}'-\vec{m})^2]\cosh[\omega_t\tilde{\beta}_l(t)]-2(\vec{k}-\vec{m})\cdot(\vec{k}'-\vec{m})\}\right\}. \quad \text{(C17)}$$

As is well known the Green function is Gaussian, so that the integral over $\vec{m}$ in Eq. (C15) can be performed exactly. The result is expanded to the second-order terms in t in the exponent, and we recover, as in the previous case, the representation Eq. (C9) for the l-dependent kernels $\tilde{\mathscr{G}}_l(s;\vec{k},\vec{k}')$. The expression for $\mathscr{P}_1$ and $\mathscr{P}_2(l)$ takes the same form as before (provided we neglect their dependence on $\vec{k}$ and $\vec{k}'$, and set $\vec{k}=\vec{k}'=\vec{k}_L$). From this point, the same analysis as the one presented above applies, and we recover Eq. (14).

[1] M. Lewenstein, L. You, J. Cooper, and K. Burnett, Phys. Rev. A **50**, 2207 (1994).

[2] L. You, M. Lewenstein, and J. Cooper, Phys. Rev. A **51**, 4712 (1995).

[3] (a) J. M. Doyle, J. C. Sandberg, I. A. Yu, C. L. Cesar, D. Kleppner, and T. J. Greytak, Phys. Rev. Lett. **67**, 603 (1991); (b) C. R. Monroe, E. A. Cornell, C. A. Sackett, C. J. Myatt, and C. E. Wieman, *ibid.* **70**, 414 (1993); (c) W. Ketterle, K. B. Davis, M. A. Joffe, A. Martin, and D. E. Pritchard, *ibid.* **70**, 2253 (1993); (d) I. D. Setija, H. G. C. Werij, O. J. Luiten, M. W. Reynolds, T. W. Hijmans, and J. T. M. Walraven, *ibid.* **70**, 2257 (1993); (e) R. J. C. Spreeuw, C. Gerz, L. S. Goldner, W. D. Phillips, S. L. Rolston, C. I. Westbrook, M. W. Reynolds, and I. F. Silvera, *ibid.* **72**, 3162 (1994).

[4] J. Opt. Soc. Am. B **6** (1989), special issue on laser cooling and trapping of atoms, edited by S. Chu and C. Wieman; S. L. Gilbert and C. E. Wieman, Opt. Photonics News **4**, 8 (1993).

[5] *Proceedings of the Fourteenth International Conference on Atomic Physics, Boulder, Colorado, 1994*, edited by D. J. Wineland, C. E. Wieman, and S. J. Smith, AIP Conf. Proc. No. 323 (AIP, New York, 1995).

[6] (a) W. Petrich, M. H. Anderson, J. R. Ensher, and E. A. Cornell (unpublished); (b) K. B. Davis, M. O. Mewes, M. A. Joffe, and W. Ketterle (unpublished); (c) S. Chu (private communication).

[7] H. F. Hess, G. P. Kochanski, J. M. Doyle, N. Masuhara, D. Kleppner, and T. J. Greytak, Phys. Rev. Lett. **59**, 672 (1987); R. van Roijen, J. J. Berkhout, S. Jaakkola, and J. T. M. Walraven, *ibid.* **61**, 931 (1988); N. Masuhara, J. M. Doyle, J. C. Sandberg, D. Kleppner, T. J. Greytak, H. F. Hess, and G. P. Kochansky, *ibid.* **61**, 935 (1988); C. Monroe, W. Swann, H. Robinson, and C. Wieman, *ibid.* **65**, 1571 (1990).

[8] I. F. Silvera and J. T. M. Walraven, in *Spin-Polarized Hydrogen*, in *Progress in Low Temperature Physics*, edited by D. F. Brewer (Elsevier, Amsterdam, 1986); J. T. M. Walraven, in *Proceedings of the Fourteenth International Conference on Atomic Physics* (Ref. [5]).

[9] B. Svistunov and G. Shlyapnikov, Zh. Éksp. Teor. Fiz. **97**, 821 (1990) [Sov. Phys. JETP **70**, 460 (1990)]; **98**, 129 (1990) [**71**, 71 (1990)].

[10] H. D. Politzer, Phys. Rev. A **43**, 6444 (1991).

[11] J. Javanainen, Phys. Rev. Lett. **72**, 2375 (1994).

[12] M. Lewenstein, L. You, and J. Cooper, in Proceedings of the International Conference on Quantum Optics III, Szczyrk, 1993, edited by M. Kolwas and J. Mostowski [special issue of Acta Phys. Polon. A **86**, 173 (1994)]; L. You, M. Lewenstein, and J. Cooper, Phys. Rev. A **50**, R3565 (1994).

[13] M. Gajda and J. Mostowski (unpublished); strictly speaking those authors consider the case of scattering of a single photon on a single atom in the trap. Such a problem is equivalent to the problem of scattering of the weak light on a sample of N atoms in the Born approximation. Analytical methods used by Gajda and Mostowski are closely related to the ones used by Stoop and Rzążewski [14] in their study of spontaneous emission from a single trapped atom, as well as to the ones used by us.

[14] H. Stoop and K. Rzążewski, Phys. Rev. A **52**, 1494 (1995).

[15] O. Morice, Y. Castin, and J. Dalibard, Phys. Rev. A **51**, 3896 (1995).

[16] M. Lewenstein and L. You, Phys. Rev. Lett. **71**, 1339 (1993).

[17] It is worth stressing the (collisional) line-shape problem for statistically indistinguishable atoms has been the subject of earlier studies; see, for instance, D. Loss, A. Thellung, and Ł. A. Turski, Phys. Rev. A **41**, 3005 (1990).

[18] J. R. Taylor, *Scattering Theory: The Quantum Theory of Nonrelativistic Collisions* (Wiley, New York, 1987).

[19] R. J. Glauber, in *Lectures in Theoretical Physics*, edited by W. E. Brittin and L. G. Dunham (Interscience, New York, 1959), Vol. I, p. 315.

[20] Applications of the GDT to the case of a potential of Gaussian shape was discussed by M. Bleszyński, R. J. Glauber, and P. Ostlund, Phys. Lett. **104**B, 389 (1981).

[21] For more recent applications of the GDT see Y. Abgrall, R. Belaidi, and J. Labarsouque, in *Coherence, Cooperation and Fluctuations*, edited by F. Haake, L. M. Narducci, and D. F. Walls (Cambridge University Press, Cambridge, 1986), p. 46; M. Bleszynski and T. Jaroszewicz, *ibid.*, p. 52; V. Franco, *ibid.*, p. 81; R. J. Lombard, *ibid.*, p. 90; C. Wilkin, *ibid.*, p. 95.

[22] See Refs. [1], [3(b)], [6(a)], [12], [16].

[23] N. N. Bogoliubov, J. Phys. Moscow **11**, 231 (1947); A. Griffin, *Excitations in a Bose-Condensed Liquid* (Cambridge University Press, Cambridge, 1993).

[24] M. Edwards and K. Burnett, Phys. Rev. A **51**, 1382 (1994); C. Myatt (private communication).

[25] L. You and M. Lewenstein (unpublished).

[26] See, for instance, code D02KDF in *NAG Manual* (NAG Inc., 1400 Opus Place, Suite 200, Downers Grove, IL 60515-5720, 1993).

[27] For a discussion of the so-called *contact term*, see, E. A. Power and S. Zienau, Philos. Trans. R. Soc. **251**, 427 (1959); as shown in Refs. [1,12] this term can be easily incorporated in the theory, although it does not seem to play a crucial role in the range of parameters considered in this paper.

[28] C. Cohen-Tannoudji, J. Dupont-Roc, and G. Grynberg, *Atoms and Photons, Introduction to Quantum Electrodynamics* (Wiley, New York, 1989).

[29] The validity of the decorrelation approximation can be studied by deriving a Fokker-Planck equation corresponding to the Heisenberg operator Eqs. (3)–(5). It can be shown that for level occupation $N_{\vec{n}} \gg 1$, the error is of order $1/\sqrt{N_{\vec{n}}}$. In addi-

tion, the overall validity is also assured by the self-consistency achieved in the solution.

[30] In doing so, we have also neglected a part of the dipole-dipole interactions related to the fluctuations of the dipole operator $\vec{d}$. The full contribution of the dipole-dipole interaction is proportional to $\propto \vec{d}\cdot\vec{d}$. Within the linearization (perturbative) approach and the decorrelation approximation we calculate only $\langle\vec{d}\rangle$. Consequently, we neglect all of the terms of the form $\langle\delta\vec{d}\cdot\delta\vec{d}\rangle$ with $\delta\vec{d}=\vec{d}-\langle\vec{d}\rangle$. The use of this approximation is therefore restricted to not too high atomic and optical densities.

[31] *Handbook of Mathematical Functions*, edited by M. Abramowitz and I. A. Stegun (Dover, New York, 1974).

[32] In Eq. (123) of paper I there is a misprint. The term proportional to $E_{\vec{n}}^{g}$ is missing in the denominator of the reduced scattering kernel.

[33] M. Lewenstein and L. You (unpublished).

[34] R. J. Ballagh and J. Cooper, J. Quantum. Spectrosc. Radiat. Transfer **23**, 535 (1980).

[35] This is a very special property of coherent wave packets in an harmonic potential. They do not diffuse. In general, in anharmonic potentials the packets undergo oscillation with superimposed diffusion, caused by the dephasing of the different components of the packets.

[36] J. H. Eberly, N. B. Narozhny, and J. J. Sanchez-Mondragon, Phys. Rev. Lett. **44**, 1323 (1980); G. Rempe and H. Walther, *ibid*. **58**, 353 (1987).

[37] P. M. Morse and H. Feshbach, *Methods of Theoretical Physics* (McGraw-Hill, New York, 1953).

[38] K. Huang, *Statistical Mechanics* (Wiley, New York, 1987); S. Flugge, *Practical Quantum Mechanics* (Springer, New York, 1974).

[39] A. L. Fetter and J. D. Walecka, *Quantum Theory of Many-Particle Systems* (McGraw-Hill, New York, 1971).

[40] S. T. Beliaev, Zh. Éksp. Teor. Fiz. **34**, 417 (1958) [Sov. Phys. JETP **7**, 289 (1958)]; see also N. M. Hugenholtz and D. Pines, Phys. Rev. **116**, 489 (1959).

[41] In fact, the self-consistent approach, termed the Hartree-Bogoliubov method, can be formulated directly within the framework the *T*-matrix approximation [see K. A. Brueckner and K. Sawada, Phys. Rev. **106**, 1117 (1957)]; alternatively, one can first derive the effective two-body potential and then treat its effects self-consistently; we adopt the latter approach in this paper.

[42] V. V. Goldman, I. F. Silvera, and A. J. Leggett, Phys. Rev. B **24**, 2870 (1981).

[43] R. H. Dicke, Phys. Rev. **89**, 472 (1953); S. G. Rautian and I. I. Sobel'man, Usp. Fiz. Nauk **90**, 209 (1966) [Sov. Phys. Usp. **9**, 701 (1967)].

[44] This can be easily seen from analyzing Eqs. (60) and (62). In the high-temperature limit, $a\rightarrow\infty$, and all the Lorentzians contributing to the sums in Eqs. (60) and (62) have a width Γ, since $\gamma_L^l \ll \Gamma$. Thus, the Lorentzian spectrum of the width Γ characterizes all partial wave components. On the other hand, at low temperature, and in the regime of parameters considered here, $\gamma_L^l \gg \Gamma$ for small l, and $\gamma_L^l \ll \Gamma$ for l larger than $\simeq k_L^2 a^2$. In the latter case, only very high partial waves contribute to the narrow feature.

[45] Both time variable t and spatial variable $\vec{R}$ are involved in treating the multiple scattering events considered here. For the time variable, in the limit $t\rightarrow\infty$, energy conservation dictates the solution to be of the type $e^{-i\omega_L t}$ for the linear scattering equation since the driving is of the same type, and monochromatic. This is equivalent to putting $s=-i\omega_L$ with respect to the Laplace variable s in both the on-shell and the GDT approximations. However, the two approximations handle the spatial propagation differently. In the on-shell approximation, the length of the $\vec{k}$ vector is fixed by the ansatz $\delta(ck-\omega_L)$ in Eq. (50). That means that the spatial propagation during successive rescattering events is dispersionless with $k=\omega_L/c$. In the GDT, $\vec{k}$ is only assumed to be close to $\vec{k}_L$; in particular, the wave vector variation $\delta\vec{k}=\vec{k}-\vec{k}_L$ might have nonzero components in the $\vec{k}_L$ direction, whereas its transverse components are set equal to zero.

[46] S. R. de Groot, G. J. Hooyman, and C. A. ten Seldam, Proc. R. Soc. London Ser. A **203**, 266 (1950).

[47] V. Bagnato, D. E. Pritchard, and D. Kleppner, Phys. Rev. A **35**, 4354 (1987).

[48] B. R. Mollow, Phys. Rev. A **12**, 1919 (1975).

[49] W. Heitler, *The Quantum Theory of Radiation* (Dover, New York, 1984).

[50] R. P. Feynman and A. R. Hibbs, *Quantum Mechanics and Path Integrals* (McGraw-Hill, New York, 1965).